

Assembly and architecture of precursor nodes during fission yeast cytokinesis

Damien Laporte,¹ Valerie C. Coffman,¹ I-Ju Lee,^{1,2} and Jian-Qiu Wu^{1,3}

¹Department of Molecular Genetics, ²Graduate Program of Molecular, Cellular, and Developmental Biology, ³Department of Molecular and Cellular Biochemistry, The Ohio State University, Columbus, OH 43210

The contractile ring is essential for cytokinesis in most fungal and animal cells. In fission yeast, cytokinesis nodes are precursors of the contractile ring and mark the future cleavage site. However, their assembly and architecture have not been well described. We found that nodes are assembled stoichiometrically in a hierarchical order with two modules linked by the positional marker anillin Mid1. Mid1 first recruits Cdc4 and IQGAP Rng2 to form module I. Rng2 subsequently recruits the myosin-II subunits Myo2 and Rlc1. Mid1 then independently

recruits the F-BAR protein Cdc15 to form module II. Mid1, Rng2, Cdc4, and Cdc15 are stable node components that accumulate close to the plasma membrane. Both modules recruit the formin Cdc12 to nucleate actin filaments. Myo2 heads point into the cell interior, where they efficiently capture actin filaments to condense nodes into the contractile ring. Collectively, our work characterizing the assembly and architecture of precursor nodes defines important steps and molecular players for contractile ring assembly.

Introduction

Cytokinesis requires coordination of cleavage site selection, assembly and constriction of a contractile ring, and targeted membrane fusion to partition a mother cell into two daughter cells (Balasubramanian et al., 2004; Barr and Gruneberg, 2007; Pollard and Wu, 2010). In animal cells, the spindle midzone, astral microtubules, or both specify where to assemble the contractile ring (Bringmann and Hyman, 2005; Barr and Gruneberg, 2007). In *Saccharomyces cerevisiae*, the division site is determined by the bud site selection machinery (Balasubramanian et al., 2004). In *Schizosaccharomyces pombe*, the anillin-like protein Mid1 provides a positional cue for cleavage site selection (Sohrmann et al., 1996). Subsequently, the contractile ring is assembled at the specified site. Contractile rings are essential for force production and for guiding membrane fusion at the cleavage site in most fungi, amoebas, and animal cells (Hales et al., 1999; Pollard and Wu, 2010). However, molecular mechanisms of the coordination of cytokinesis stages remain elusive.

The fission yeast *S. pombe* is a favorite model for the study of cleavage site selection and contractile ring assembly (Mishra and Olierenko, 2008; Roberts-Galbraith and Gould, 2008;

Bathe and Chang, 2010). In *S. pombe*, the current model of cytokinesis proposes cytokinesis nodes as precursors of the contractile ring (Wu et al., 2006; Vavylonis et al., 2008). Although interphase nodes are essential for coordination of cell size control and the cell cycle (Martin and Berthelot-Grosjean, 2009; Moseley et al., 2009), deletion of the *cdr2* kinase, the organizer of interphase nodes, does not obviously affect the cytokinesis nodes and contractile ring formation, suggesting that these nodes can assemble independently (Almonacid et al., 2009; Moseley et al., 2009).

Cytokinesis nodes contain at least seven conserved proteins that assemble independently of actin filaments: Mid1, myosin-II heavy chain Myo2, essential light chain Cdc4, regulatory light chain Rlc1, formin Cdc12, IQGAP Rng2, and F-BAR protein Cdc15 (Pollard and Wu, 2010). Except for Mid1 and Rlc1, these proteins are essential for contractile ring assembly and/or maturation. Mid1 was reported to recruit Myo2 to nodes by interacting with the Myo2 tail (Motegi et al., 2004). Myosin-II is a hexamer composed of Myo2, Cdc4, and Rlc1, which produces a force to condense nodes into a contractile ring as well as to constrict the ring (Lord and Pollard, 2004; Vavylonis et al., 2008).

Correspondence to Jian-Qiu Wu: wu.620@osu.edu

Abbreviations used in this paper: IP, immunoprecipitation; Lat-A, latrunculin A; mECitrine, monomeric enhanced Citrine; mEGFP, monomeric EGFP; mYFP, monomeric YFP; ROI, region of interest; SCPR, search, capture, pull, and release; SHREC, single-molecule high resolution colocalization; SIN, septation initiation network; SPB, spindle pole body; tdTomato, tandem Tomato; wt, wild type.

© 2011 Laporte et al. This article is distributed under the terms of an Attribution-Noncommercial-Share Alike-No Mirror Sites license for the first six months after the publication date (see <http://www.rupress.org/terms>). After six months it is available under a Creative Commons License (Attribution-Noncommercial-Share Alike 3.0 Unported license, as described at <http://creativecommons.org/licenses/by-nc-sa/3.0/>).

Myo2 directly interacts with Cdc4 and Rlc1 through its two IQ domains at the neck region (Motegi et al., 2000; Naqvi et al., 2000), which connects an N-terminal ATPase motor domain and an α -helical tail. Formin Cdc12 nucleates linear actin filaments for the contractile ring (Kovar et al., 2003; Coffman et al., 2009). IQGAP Rng2 is essential for bundling and arranging actin filaments into the contractile ring (Takaine et al., 2009). Rng2 also interacts with Cdc4 as revealed by immunoprecipitation (IP; D'souza et al., 2001), most likely via its multiple IQ domains. F-BAR protein Cdc15 interacts with formin Cdc12 (Carnahan and Gould, 2003) and is essential for ring maturation and the Mid1-independent ring assembly (Wu et al., 2003; Wachtler et al., 2006; Hachet and Simanis, 2008).

Mid1, the first protein to appear in cytokinesis nodes (Paoletti and Chang, 2000; Wu et al., 2003), is essential for division site specification, as loss of Mid1 results in the loss of cytokinesis nodes and, thus, randomly placed contractile rings (Sohrmann et al., 1996; Wu et al., 2006). However, it was poorly understood how Mid1 recruits other proteins to form functional cytokinesis nodes and a contractile ring. The relative simplicity of cytokinesis nodes makes them an ideal structure to determine interactions and architecture of these proteins, which will provide insights into the assembly and function of the more complex contractile ring.

Here, we study the Mid1-dependent node assembly during fission yeast cytokinesis. We systematically determine localization dependencies of node proteins, their molecular stoichiometry, protein dynamics *in vivo*, and their physical interactions. In addition, we have determined the node architecture at a nanometer resolution using single-molecule high resolution colocalization (SHREC). We find that cytokinesis nodes are assembled stoichiometrically in a hierarchical order through two Mid1-dependent modules. Both modules recruit formin Cdc12 to nucleate actin filaments. Moreover, the defined node architecture provides strong support for the proposed mechanism of contractile ring assembly.

Results

In this study, we define the separation of spindle pole bodies (SPBs) labeled with Sad1-CFP, which marks the initiation of mitosis, as time 0. We define cytokinesis nodes as discrete protein clusters (20–65) close to the equatorial plasma membrane during the G2/M transition.

Cdc4 and IQGAP Rng2 localize to cytokinesis nodes independently of Myo2

To investigate the assembly of cytokinesis nodes, we first tested whether the myosin-II heavy chain Myo2 recruits its light chains Rlc1 and Cdc4 and IQGAP Rng2 to the nodes through its two IQ domains. Deletion of the IQ domains prevents the interactions between Myo2 and its light chains (Naqvi et al., 2000; D'souza et al., 2001). In wild-type (wt) cells at 25°C, a broad band of Rlc1, Cdc4, and Rng2 nodes appeared at the cell equator at similar times (Fig. 1 A, left). In *myo2-IQ1ΔIQ2Δ* cells with both IQ domains deleted, Cdc4 and Rng2 nodes still appeared with normal timing (Fig. 1 A, right). The contractile ring

also formed normally as previously reported (Naqvi et al., 2000). In contrast, no Rlc1 nodes were observed, and Rlc1 localization to the ring was significantly delayed. In this background, Rlc1 ring localization depends on Myp2 (Naqvi et al., 2000; Wu et al., 2003). Thus, Rlc1, but not Cdc4 or Rng2, depends on the IQ domains of Myo2 for localization to cytokinesis nodes.

To find whether other domains of Myo2 are required for Cdc4 and Rng2 localization to cytokinesis nodes, we examined protein localization in *myo2Δ* cells (see Materials and methods). The maternal contribution of Myo2 was negligible because we observed no monomeric YFP (mYFP)-Myo2 signal in *myo2Δ* cells at any cell cycle stage, and Rlc1 localized to a clump instead of to nodes or a contractile ring (Fig. S1, A and B). In contrast, Cdc4 and Rng2 nodes were observed in *myo2Δ* cells (Fig. 1 B and Table I). However, \sim 10 min after their appearance, the nodes began to clump. These results were confirmed using an *N-degron-myo2* strain (Fig. S1, C and D). In summary, Myo2 is critical for node condensation into a contractile ring and for Rlc1 node localization. However, it is not required for Cdc4 and Rng2 localization to cytokinesis nodes.

Myo2 node localization depends on both Cdc4 and Rng2

We next investigated whether Myo2 depends on Rlc1, Cdc4, or Rng2 for localization to cytokinesis nodes. Rlc1 deletion did not affect node localization of Myo2 or other node proteins (Fig. S1 E). In contrast, Cdc4 and Rng2 were required for Myo2 localization to nodes. In wt cells at 36°C, Myo2 appeared in nodes at -6.1 ± 1.9 min ($n = 30$ cells; Fig. 1 C). Although the protein level of Myo2 was not obviously affected by the *cdc4-8* or *rng2-D5* mutation (see Fig. 5 B and Fig. S2 A, middle), no Myo2 accumulated in nodes in temperature-sensitive *cdc4-8*, *rng2-D5*, or *rng2-346* mutants ($n > 35$ cells for each) at 36°C nor in *cdc4Δ*- and *rng2Δ*-null mutants at 25°C (Fig. 1, C and D; and not depicted). In *cdc4-8* cells at 5–7 min, Myo2 appeared as faint structures (Fig. 1 C) that either aggregated into clumps or disappeared. We observed no Myo2 structures after latrunculin A (Lat-A) treatment (Fig. S2 B), indicating that these structures are actin dependent, unlike nodes (Wu et al., 2006). In *rng2* mutants, all cells formed a clump at 6–7 min (Fig. 1, C and D). The same genetic dependency was found for Rlc1 (Fig. S2 D and not depicted). Together, these results indicate that Myo2 and Rlc1 node localization depends on both Rng2 and Cdc4.

Cdc4 and Rng2 are interdependent for node localization, and both affect Mid1 levels in cytokinesis nodes

To better understand how Myo2 is recruited to cytokinesis nodes, we investigated whether the interaction between Cdc4 and Myo2 is required for Myo2 node localization. Cells expressing mYFP-Myo2-IQ1ΔIQ2Δ formed nodes at -4.1 ± 2.1 min ($n = 63$ cells) and normal contractile rings at 36°C, similar to wt mYFP-Myo2 (-3.9 ± 1.7 min; $n = 29$; Fig. 2 A). Because Myo2-IQ1ΔIQ2Δ cannot interact with Cdc4 (D'souza et al., 2001), this result suggests that Myo2 can localize to cytokinesis nodes independently of Cdc4, which seems to conflict with our

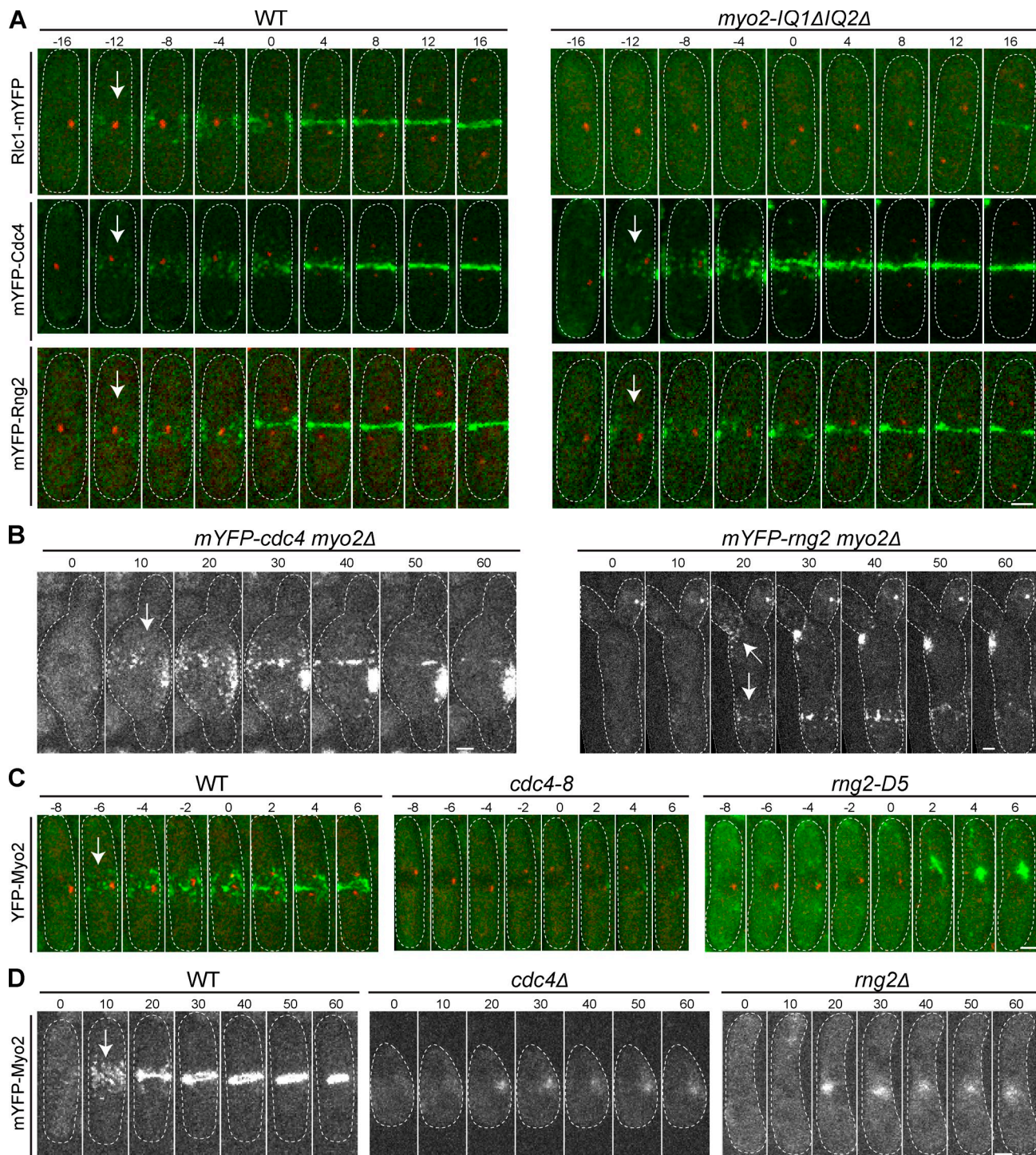


Figure 1. Myo2 localization to cytokinesis nodes depends on both Cdc4 and Rng2. (A) Rlc1, but not Cdc4 and Rng2, depends on IQ domains of Myo2 for node localization. Time courses of Rlc1-mYFP, mYFP-Cdc4, and mYFP-Rng2 localization in asynchronous wild type (WT) and the *myo2*-*IQ1Δ/Q2Δ* mutant at 25°C ($n > 20$ cells for each). (B) Localization of Cdc4 ($n = 11$ cells) and Rng2 ($n = 16$) in *myo2*Δ after growing for 24 h at 25°C. (C) Time courses of the localization of Myo2 in temperature-sensitive *cdc4* and *rng2* mutants ($n > 35$ cells for each) at the restrictive temperature 36°C (see Materials and methods). (D) Time courses of the localization of Myo2 in *cdc4*Δ and *rng2*Δ ($n > 10$ cells for each) after growing for 12 h at 25°C. The cell boundary is marked with dashed lines; elapsed times on micrographs are in minutes; arrows indicate node appearance; the SPB separation (Sad1-CFP, red) is defined as time 0; the time 0 on micrographs without Sad1-CFP is relative. Bars, 2 μ m.

findings that Myo2 failed to localize to nodes in *cdc4*-8 and *cdc4*Δ mutants (Fig. 1, C and D). Thus, we hypothesized that Cdc4 recruits a protein that in turn helps recruit Myo2 to cytokinesis nodes.

It has been suggested that Mid1 recruits Myo2 to nodes (Motegi et al., 2004). One explanation for our data, therefore, could be that *cdc4* and *rng2* mutations affect Mid1 localization in nodes so that Myo2 fails to localize properly. In cells

Table I. Genetic dependencies of protein localization to cytokinesis nodes

Node protein	wt ^{a,b}	No F-actin ^{a,b,c}	mid1 ^d	rng2 ^e	cdc4 ^f	myo2 ^g	rlc1 ^h	cdc15 ⁱ	cdc12 ^j
Mid1	++ - ^{e,f}	+- - ^f		+- -	+- -	ND	ND	++ -	+- -
Rng2	++ -	+- -	- + - ^b		-- - ^b	+- +	++ -	++ -	+- - ^b
Cdc4	++ -	+- -	- + -	-- +		+- +	++ -	++ -	+- -
Myo2	++ - ^g	+- - ^{g,h}	- + - ^b	-- +	-- + ^g		++ -	++ -	+- - ^g
Rlc1	++ - ⁱ	+- -	- + - ⁱ	-- +	-- +	-- + ^k		++ - ^l	ND
Cdc15	++ -	+- -	- + - ^{a,j}	+- +	+- +	+- +	++ -		+- -
Cdc12	++ - ^m	+- -	- + - ^{j,m}	+- +	+- +	ND	++ -	++ -	

Localization under test conditions. Data is given as node, ring, and clump, respectively. Except for *rlc1*, both null and temperature-sensitive mutants were tested, and the same results were obtained. Italic +/− indicates the genetic dependencies tested in this study; non-italic +/− indicates the published genetic results not tested in this study. Because our experiments focus on the node assembly, the published genetic dependencies on ring and clump formation were not cited here.

^aWu et al., 2006.

^bWu et al., 2003.

^cLatA treatment.

^dIn the absence of Mid1, cytokinesis nodes do not form. After a delay, cells usually assemble a contractile ring that is generally mislocalized and constricts slowly (Wu et al., 2003; Hachet and Simanis, 2008; Huang et al., 2008).

^eSohrmann et al., 1996; Bähler et al., 1998a.

^fPaoletti and Chang, 2000.

^gMotegi et al., 2000: no Myo2 signal was detected in the *cdc4* temperature-sensitive strain. But in our study, we show that Myo2 localizes as a faint disorganized structure.

^hMulvihill et al., 2001.

ⁱLe Goff et al., 2000.

^jHuang et al., 2008.

^kNaqvi et al., 2000.

^lHachet and Simanis, 2008.

^mCoffman et al., 2009.

from germinated wt, *cdc4Δ*, and *rng2Δ* spores, Mid1 localized in the nucleus during interphase and then exited from the nucleus and formed nodes (Fig. 2 B). Mid1 stayed in nodes for ~30 min in the deletion strains before moving back to the daughter nuclei without forming a contractile ring or clumps. Mid1 localized in nodes with ~25% lower fluorescence intensity in *cdc4-8 cdr2Δ* than in *cdr2Δ*, although the Mid1 concentration in cells was the same (Fig. 2, C and D). Similar reduction was observed in *rng2-D5*, *cdc4Δ*, and *rng2Δ* cells. Thus, our data suggest that Cdc4 and Rng2 affect Mid1 accumulation to nodes. However, the partial reduction in Mid1 level alone cannot explain the complete lack of Myo2 nodes in *cdc4* and *rng2* mutants.

Rng2 is required for Myo2 node localization (Fig. 1, C and D) and interacts with Cdc4 through its multiple IQ domains (D'souza et al., 2001). To ask whether Myo2 could depend on Rng2 in *cdc4* mutants, we investigated Rng2 localization in *cdc4-8* (Fig. 2 E) and in *cdc4Δ* cells. At 36°C, no Rng2 nodes, clumps, or rings were observed in dividing cells ($n = 20$ cells), although Rng2 protein level was not affected by the *cdc4-8* mutation (Fig. S2 A, left). The same results were obtained in *cdc4Δ* cells at 25°C (unpublished data). Next, we investigated the dependency of Cdc4 localization on Rng2. Similar to Myo2 and Rlc1, Cdc4 formed no nodes or rings but formed a clump in *rng2-D5*, *rng2-346*, or *rng2Δ* cells (Fig. 2 F and not depicted), whereas Cdc4 protein level was not obviously affected in *rng2-D5* (Fig. S2 A, right). Collectively, these results suggest that Cdc4 and Rng2 are interdependent for node localization and help clarify how Myo2 accumulation depends on the presence of Cdc4.

F-BAR protein Cdc15 depends on Mid1 for localization to cytokinesis nodes

We next addressed which node protein is required for Cdc15 localization to cytokinesis nodes. In wt cells at 36°C, Cdc15 localized to nodes at 0.9 ± 1.3 min ($n = 21$ cells). Surprisingly, all *cdc4-8*, *rng2-D5*, and *rng2-346* dividing cells displayed Cdc15 nodes. The nodes appeared later than in wt (3.7 ± 2 min; $n = \sim 30$ cells each) and aggregated into clumps instead of forming a contractile ring (Fig. S2 C and not depicted). Furthermore, Cdc15 still localized to cytokinesis nodes in *cdc4Δ* and *rng2Δ* cells (Fig. 3 A).

The delayed appearance of Cdc15 in nodes in *cdc4* and *rng2* mutants may result from the reduced Mid1 levels in nodes (Fig. 2, B–D). Indeed, we detected no Cdc15 nodes in *mid1Δ* cells, although Cdc15 still concentrated at endocytic patches and a mislocalized and tilted ring (Fig. 3 A). Conversely, the Mid1 level in nodes was not affected in *cdc15* mutants. Collectively, these results suggest that Cdc15 localization to nodes depends only on Mid1.

Cdc4 and Rng2 node localization are independent of Cdc15

Cdc15 localization to cytokinesis nodes is independent of Cdc4 and Rng2 (Fig. 3 A). We explored whether Cdc15 plays a role in the accumulation or maintenance of Cdc4 and Rng2 to nodes using *cdc15* mutants. We detected no mYFP-Cdc15 signals in *cdc15Δ* cells (Fig. S3 A), suggesting a negligible maternal contribution of Cdc15. Cdc4 and Rng2 nodes were observed in *cdc15Δ* cells (Fig. S3, B and C; and Table I). These nodes condensed slowly into an unstable ring that collapsed before its disappearance. It took

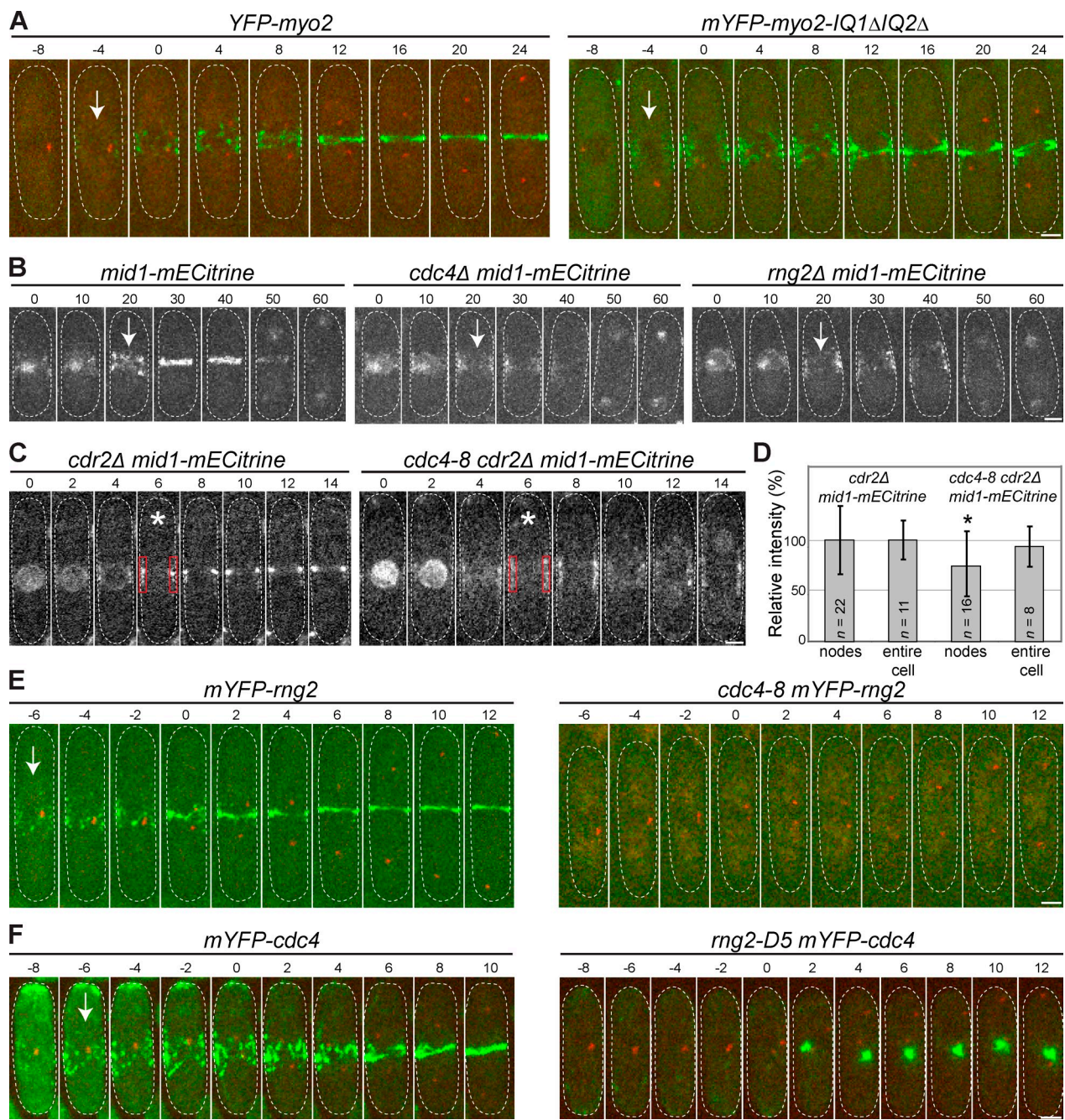


Figure 2. Cdc4 and Rng2 localizations are interdependent and both affect Mid1 levels in cytokinesis nodes. (A) Myo2 does not depend on its direct interaction with Cdc4 for node localization. Time courses of localization of Myo2 and Myo2-IQ1 Δ /IQ2 Δ at 36°C. Note that these strains are *ura4*⁺ and grow faster than *ura4-D18* cells. (B) Mid1 forms nodes with lower intensity in *cdc4 Δ* and *rng2 Δ* cells after growing for 12 h at 25°C. Arrows indicate that Mid1 is in cytokinesis nodes just after it disappears from the nucleus. (C) Single focal plane of Mid1 cytokinesis nodes with lower intensity in *cdc4-8 cdr2 Δ* cells. In *cdr2 Δ* cells, interphase nodes are not detectable. Asterisks indicate the frame used to quantify the node fluorescence intensity. Red boxes indicate the areas used to measure node intensity. (D) Mid1 concentration in cytokinesis nodes, but not in whole cells, is significantly reduced in *cdc4-8 cdr2 Δ* cells. Fluorescence intensity (mean \pm SD) of whole cells or within a box of $0.7 \times 3.5 \mu\text{m}^2$ over nodes as indicated in C was measured. The asterisk indicates statistical difference. (E) Cdc4 is required for Rng2 localization to the nodes. Time courses of Rng2 in wt and *cdc4-8* at 36°C. (F) Rng2 is required for Cdc4 localization to the nodes. Time courses of Cdc4 in wt and *rng2-D5* at 36°C. The cell boundary is marked with dashed lines; elapsed times on micrographs are in minutes; arrows indicate node appearance; the SPB separation (Sad1-CFP, red) is defined as time 0; the time 0 on micrographs without Sad1-CFP is relative. Bars, 2 μm .

~15 min for Cdc4 node condensation into a ring in *cdc15 Δ* cells ($n = 11$) compared with ~10 min in wt cells ($n = 18$). In addition, Myo2 also localized to nodes normally in *cdc15-140* cells at 36°C (Fig. S3 D). Thus, Cdc15 is not required for the accumulation or maintenance of Cdc4, Rng2, or Myo2 in cytokinesis nodes.

Formin Cdc12 is targeted to cytokinesis nodes through overlapping pathways

We next tested dependencies for Cdc12 localization to cytokinesis nodes. We found Cdc12 nodes in *rng2 Δ* , *cdc4 Δ* , and *cdc15 Δ* cells (Fig. 3 B). However, the mean fluorescence intensity

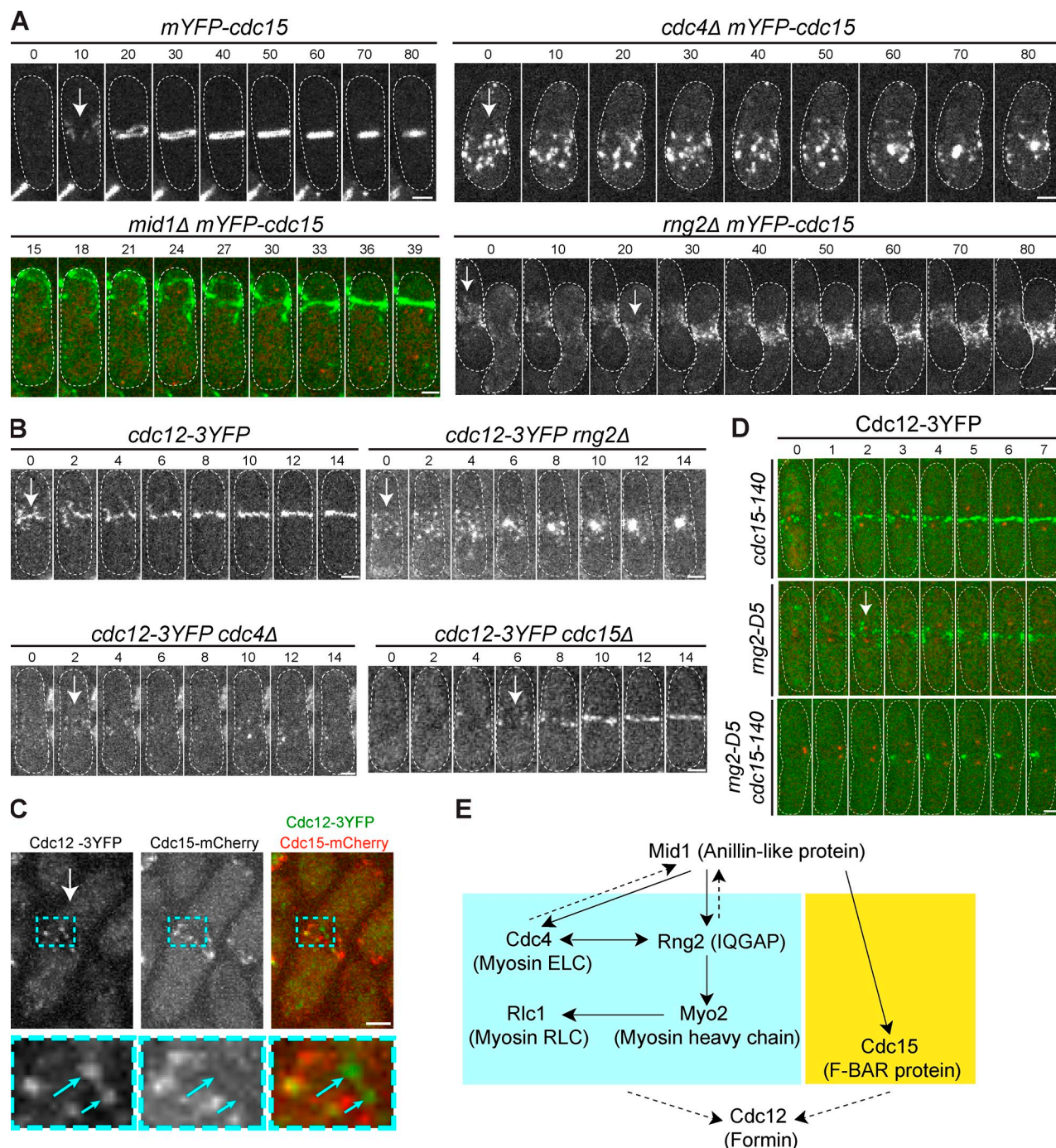


Figure 3. Genetic dependencies for node localization of Cdc15 and Cdc12 and node assembly pathways. (A) Cdc15 node localization depends on Mid1 but not on Cdc4 or Rng2. Time courses of Cdc15 localization in wt, *cdc4Δ* ($n = 28$ cells), *mid1Δ*, and *rng2Δ* ($n = 17$ cells) after 12 h at 25°C. (B) Cdc12 localizes to nodes in *rng2Δ* ($n = 17$ cells), *cdc4Δ* ($n = 10$), and *cdc15Δ* ($n = 16$) after growing for 12 h at 25°C. (C) Cdc12 partially colocalizes with Cdc15 in nodes. The boxed regions are enlarged (bottom), and blue arrows indicate Cdc12 nodes containing no Cdc15. (D) Time courses of Cdc12 localization in *cdc15-140*, *rng2-D5*, and *mg2-D5 cdc15-140* mutants after 1 h at 30°C. (E) The localization hierarchy for cytokinesis node assembly. The complete and partial dependencies of node localization on a specific protein are depicted by solid and dashed lines, respectively. The two modules are colored differently. The cell boundary is marked with dashed white lines; elapsed times on micrographs are in minutes; arrows indicate node appearance; the SPB separation (Sad1-CFP, red) is defined as time 0; the time 0 on micrographs without Sad1-CFP is relative. ELC, essential light chain. RLC, regulatory light chain. Bars, 2 μ m.

of Cdc12-3YFP nodes was \sim 40% lower in each mutant than in wt cells ($P < 10^{-4}$ each compared with wt). In addition, only 37% of Cdc12 nodes (or clusters of nodes) contained Cdc15 in wt cells ($n = 350$ Cdc12 nodes; Fig. 3 C), which indicates that Cdc12 can localize or be maintained in nodes without Cdc15.

Furthermore, Cdc12 nodes were not detected in *mg2-D5 cdc15-140* cells at the semipermissive temperature of 30°C, whereas they were in the single mutants ($n = 23$ cells; Fig. 3 D). These data suggest that Cdc4–Rng2 and Cdc15 have an overlapping function in recruiting formin Cdc12 to cytokinesis nodes.

On the other hand, Rng2, Myo2, Cdc15, and Mid1 localized to nodes, but not clumps, in *cdc12Δ* cells (Fig. S3, E–H; and Table I), suggesting that Cdc12 is downstream of other node proteins in the localization hierarchy and is required for clump formation.

We hypothesized that the clumping observed in *rng2-D5* mutants may represent failed ring formation as predicted by the search, capture, pull, and release (SCPR) model (Vavylonis et al., 2008). Consistent with this hypothesis, Cdc15, Rlc1, and Cdc12 colocalized with Myo2 in clumps in *rng2-D5* cells (Fig. S2, C–E). Furthermore, clump formation and stability depended on actin filaments, as revealed by Lat-A treatment (Table I).

In summary of the localization dependencies, we proposed two modules through which cytokinesis nodes are assembled hierarchically (Fig. 3 E). Module I consists of Mid1 recruiting Cdc4 and Rng2, which subsequently recruits Myo2 and Rlc1. Cdc4 and Rng2 provide a positive feedback on Mid1 recruitment. Module II assembles independently and consists of Mid1 recruiting Cdc15. Both modules are involved in recruiting formin Cdc12.

Temporal pathway and stoichiometry of node assembly

We hypothesized that proteins upstream in our localization hierarchy (Fig. 3 E) should appear earlier in the nodes. Thus, we quantified the timing of node appearance and absolute protein levels of the seven node proteins (see Materials and methods) with high resolution (Fig. 4 A and Table II). Consistent with its scaffolding role, interphase nodes each accumulated \sim 17 Mid1 molecules well before cytokinesis nodes appeared as indicated by the first plateau (from greater than -15 to -12.5 min; Fig. 4 A). At -10 min, Mid1 levels reached a second plateau of 28 molecules per cytokinesis node.

Supporting the localization hierarchy, we observed that Cdc4 and Rng2 appeared in nodes earlier than Myo2 and Rlc1. The accumulation of Cdc4 and Rng2 was biphasic, and that of Myo2–Rlc1 was monophasic. Cdc4 and Rng2 nodes appeared with similar timing at -11.9 ± 1.4 min and -12.5 ± 1.1 min, respectively ($P = 0.9$; Fig. 4 A, arrows). The numbers of molecules in each node (134 for Cdc4 and 9 for Rng2) remained constant until -5 min, defining the first plateau. The molecule numbers then increased to 286 and 28, respectively, reaching the second plateau at SPB separation (time 0; Fig. 4 A).

Myo2 and Rlc1 displayed almost constant molecular levels (55 for Myo2 and 41 for Rlc1) after the last node formed (Fig. 4 A). These two proteins appeared in nodes later than Cdc4–Rng2, at -10.2 ± 2.5 min and -10.2 ± 1.8 min, respectively (Fig. 4 A, arrow). These times are statistically different from those measured for Cdc4 and Rng2 ($P < 0.05$, comparing the timing of Cdc4 or Rng2 to Myo2 or Rlc1). Consistent with the timing, $>50\%$ of Cdc4 nodes had no Rlc1 during node appearance (Fig. 4, B and C). In contrast, Myo2 and Rlc1 always colocalized in nodes regardless of the number of nodes at the cell equator (Fig. 4, B and C). These results suggest that Rng2 and Cdc4 are the first proteins localized to cytokinesis nodes after Mid1. Cdc15 appeared in nodes later than module I at -4.9 min with 36 molecules at the plateau, and Cdc12 appeared last in nodes at 1 min with approximately six to eight molecules

in each node (Fig. 4 A), which is consistent with the localization hierarchy (Fig. 3 E).

FRAP analysis indicates that node proteins display different dynamics

Scaffolding proteins are usually more stable components of protein complexes. Many proteins are known to be very dynamic in contractile rings (Pelham and Chang, 2002; Clifford et al., 2008; Roberts-Galbraith et al., 2009), but little is known about their stabilities within cytokinesis nodes. We used FRAP to test the proposed pathways for node assembly (Fig. 3 E). Mid1 recovered slowly in nodes after photobleaching with a half-time of 3.03 min (Fig. 4 D and Table II), which is consistent with its scaffolding function.

The recovery of Cdc4 in nodes after photobleaching was biphasic, with a fast ($t_{1/2} = 0.20$ min) and a slow (1.45 min) recovery phase (Fig. 4 E). The fast phase depended on Cdc4's interaction with Myo2, as it was lost in the *myo2-IQ1ΔIQ2Δ* strain ($t_{1/2} = 1.39$ min; Fig. 4, E and G). In addition, Rng2 was not very dynamic in nodes, with a recovery half-time of 1.77 min in wt and 1.39 min in the *myo2-IQ1ΔIQ2Δ* mutant; the latter is identical to the slow phase of Cdc4 (Fig. 4, F and G). In contrast, Myo2 and Rlc1 were highly dynamic in the nodes with a similar recovery half-time (0.51 min) and extent of recovery (Fig. 4 H and Table II).

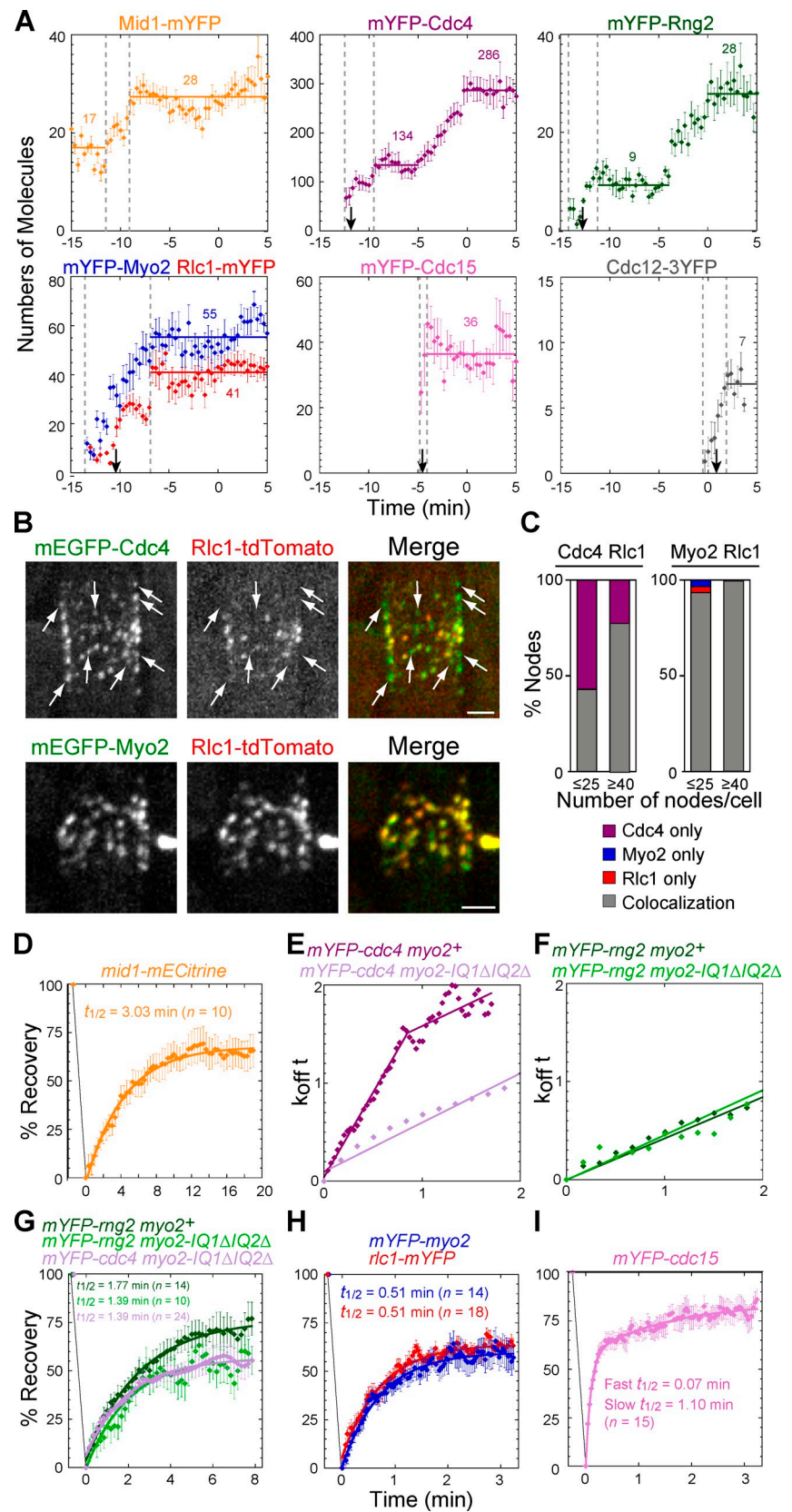
Recovery of Cdc15 in nodes after photobleaching was biphasic, with a fast ($t_{1/2} = 0.07$ min) and a slow ($t_{1/2} = 1.10$ min) phase (Fig. 4 I). Previously, we have shown that Cdc12 is dynamic in the nodes ($t_{1/2} = 0.5$ min; Coffman et al., 2009). In summary, the FRAP experiments suggest that Mid1, Cdc4, Rng2, and Cdc15 are scaffolding proteins that recruit more dynamic components Myo2, Rlc1, and Cdc12 to the nodes, which is consistent with the localization hierarchy (Fig. 3 E).

Physical interactions among cytokinesis node proteins

To further test the node-assembly pathway (Fig. 3 E), we investigated some of the key physical interactions among the node proteins. Mid1 coimmunoprecipitated with both Cdc4 and Rng2 (Fig. 5 A) from lysates of asynchronous cultures. Reciprocal co-IPs confirmed the interactions (unpublished data). In contrast, co-IP between Myo2 and Mid1 was not as efficient, even though more Myo2 than Rng2 was present (Fig. 5 A). As a negative control, Mid1 did not coimmunoprecipitate with Rlc1 under the same conditions (unpublished data). Interestingly, Mid1 did not coimmunoprecipitate with Myo2 in extracts from *rng2-D5* cells grown at 36°C (Fig. 5 B). This suggests that the physical interaction between Myo2 and Mid1 depends on Rng2 in nodes and/or in the contractile ring. Indeed, Myo2 coimmunoprecipitated with both Rng2 and Cdc4 (Fig. 5 C). Actin filaments were not involved in the Myo2–Mid1 and Myo2–Rng2 physical interactions we observed because we detected no actin after IP (Fig. S2 F and not depicted).

Previous data (D'souza et al., 2001) and ours (Figs. 2, E and F; and 4, A and E–G) suggest that Cdc4 and Rng2 may directly interact with each other. Indeed, they interacted in yeast two-hybrid assays, and the interaction was lost in budding yeast cells expressing Cdc4-8 at restrictive temperatures (Fig. 5 D).

Figure 4. Temporal pathway, stoichiometry, and dynamics of node assembly. (A) Counting node proteins over time reveals that Cdc4 and Rng2 localize to nodes before Myo2, Rlc1, Cdc15, and Cdc12. Time 0 represents the SPB separation. Colored dots are the mean numbers of molecules observed at a specific time point. Myo2 and Rlc1 are in the same graph for comparison. The dashed lines represent the time span of the appearance of individual nodes. The arrows indicate the mean timing for node appearance. The mean number of molecules at each plateau (marked by the horizontal lines) is shown in the graph. (B and C) Cdc4 does not always colocalize with Rlc1 at the beginning of node appearance. (B) Strains expressing mEGFP-Cdc4 Rlc1-tdTomato (top) and mEGFP-Myo2 Rlc1-tdTomato (bottom) were imaged at 25°C. The arrows indicate Cdc4 nodes containing no Rlc1. Bars, 1.5 μ m. (C) Quantification of the percentage of colocalization in nodes as a function of node numbers in cells for strains expressing mEGFP-Cdc4 Rlc1-tdTomato (left graph) and mEGFP-Myo2 Rlc1-tdTomato (right graph). More than 100 nodes were counted for each bar. (D–I) Fluorescence recovery curves after photobleaching in the strains indicated at the top of the graphs. Each color represents a different strain. Half-times and numbers of analyzed cells are indicated. (D and G–I) Percentage recovery is depicted on the y axis. (E and F) $k_{off} \times t$ is plotted as a function of time (in minutes) to illustrate the biphasic/monophasic recovery rate (slope). Error bars are SEM.



Based on the localization hierarchy (Fig. 3 E), we proposed that Mid1 directly recruits Cdc15 to cytokinesis nodes. Consistent with this hypothesis, Cdc15 interacted with itself and with Mid1 in yeast two-hybrid assays (Fig. 5 E). Moreover, Mid1

coimmunoprecipitated with Cdc15 (Fig. 5 F). Together, the aforementioned data suggest that Mid1 may directly recruit Cdc4–Rng2 and Cdc15 to cytokinesis nodes, and Rng2 recruits Myo2 or stabilizes the Myo2–Mid1 interaction in nodes.

Table II. Node protein dynamics revealed by FRAP and numbers of molecules in nodes

Genotype	Half-time, fast/slow phase (number of cells)	Recovery, fast/slow	Molecules (polypeptides) per node, first/second plateau (number of nodes)	Timing of node appearance (number of nodes)
<i>mid1-mYFP</i>	min ND	% ND	17.1 ± 7.4 (4)/ 27.7 ± 10 (23)	min -11.2 ± 1.1 (9)
<i>mid1-mECitrine</i>	3.03 ± 1.32 (10)	68.6	ND	ND
<i>mid1-mECitrine cdr2Δ</i>	1.97 ± 0.77 (10)	57.8	ND	ND
<i>mYFP-rng2</i>	1.77 ± 1.07 (14)	75.4	9.4 ± 5.6 (25)/ 28.0 ± 16.9 (25)	-12.5 ± 1.1 (8)
<i>mYFP-rng2 myo2-IQ1ΔIQ2Δ</i>	1.39 ± 0.82 (10)	56.7	10.3 ± 3.4 (16)/ 30.3 ± 9.4 (16) ^a	-12.8 ± 1.0 (16) ^a
<i>mYFP-rng2 cdr2Δ</i>	1.29 ± 0.69 (14)	57.0	ND	ND
<i>mYFP-cdc4</i>	0.20 ± 0.14/ 1.45 ± 0.45 (11)	21.1/22.3	134.1 ± 93.9 (29)/ 286.3 ± 130.4 (29)	-11.9 ± 1.4 (11)
<i>mYFP-cdc4 myo2-IQ1ΔIQ2Δ</i>	NA/1.39 ± 0.89 (24)	NA/53.4	107.5 ± 59.7 (16)/ 265.0 ± 90.1 (16) ^a	-11.4 ± 1.5 (16) ^a
<i>mYFP-myo2</i>	0.51 ± 0.22 (14)	59.5	55.3 ± 32.8 (31)	-10.2 ± 2.5 (9)
<i>mYFP-myo2-IQ1ΔIQ2Δ</i>	0.48 ± 0.31 (18)	71.4	ND	ND
<i>mYFP-myo2 cdr2Δ</i>	0.52 ± 0.22 (11)	79.7	ND	ND
<i>rlc1-mYFP</i>	0.51 ± 0.22 (18)	61.9	41.3 ± 23 (31)	-10.2 ± 1.8 (14)
<i>mYFP-cdc15</i>	0.07 ± 0.02/ 1.10 ± 0.67 (15)	57.3/27.3	36.3 ± 16.9 (21)	-4.9 ± 0.6 (12)
<i>mYFP-cdc15 cdr2Δ</i>	0.08 ± 0.04/ 0.83 ± 0.62 (15)	50.9/49.1	ND	ND
<i>cdc12-3YFP^b</i>	0.50 ± 0.17 (11)	69.3	6.9 ± 2.9 (16)	1.0 ± 0.6 (16)

Timing of node appearance is relative to the SPB separation, which is defined as time 0. The timing for Mid1 represents the timing that the Mid1 level reaches the cytokinesis node plateau. NA, not applicable.

^aNot statistically different from wt.

^bCoffman et al., 2009.

Architecture of cytokinesis nodes determined by SHREC

Our experiments of node architecture provide further support for the node-assembly pathways (Fig. 3 E). Cytokinesis nodes are separated by 558 ± 138 nm before node condensation ($n = 40$ distances measured between centroids of different Rlc1 nodes). To further investigate node assembly, we used SHREC (Churchman et al., 2005; Joglekar et al., 2009) to determine the relative positions and distances of the seven node proteins within the same nodes. The imperfect alignment of two laser channels introduces an offset (Fig. S4 A), but our method has an accuracy of ~ 10 nm after offset correction (Fig. S4, B and C). Because of the difficulties in measuring small distances using the maximum likelihood method, the longer distances we measured might be more accurate than the shorter ones (see Materials and methods). We measured two distances at right angles to each other at cell sides and cell top/bottom as indicated (Fig. 6 A). Then, the 2D distances (hypotenuses) were calculated.

To decipher node architecture, we first determined the distance and orientation of Rlc1 to the plasma membrane marked with GFP-Psy1 (GFP at the N terminus of Psy1), a t-SNARE protein that inserts into the plasma membrane through its C terminus (Sutton et al., 1998). Rlc1 binds to the neck of Myo2 through IQ domain 2 (Naqvi et al., 2000). Using SHREC, we found that the distance between Rlc1 and Psy1 is 61 nm (Figs. 6 B and S4 D). Given the sequence conservation of t-SNARE family proteins, we hypothesize that Psy1 is ~ 10 nm in length, as measured for the mammalian homologue by crystallography

(Sutton et al., 1998). Thus, we propose that Rlc1 is in the cytoplasm at ~ 70 nm from the plasma membrane.

Comparing the centroids of two protein clusters in the same nodes, we discovered that all node proteins except Myo2 are located closer to the plasma membrane than Rlc1 (Figs. 6, C–H; and S4 E). The C terminus of Myo2 is closer to the membrane than Rlc1 (Fig. 6 G), whereas the N terminus of Myo2 is further (Fig. 6, E and F), suggesting that the Myo2 head is oriented toward the cell interior.

We measured the distance between Rlc1 and the C terminus of Mid1 and determined that the 2D distance is 71 nm (Fig. 6 C). Mid1 is associated with the plasma membrane (Celton-Morizur et al., 2004). If we assume the plasma membrane is parallel to the cell's long axis, the axis of Rlc1-Mid1 is at 71° to the plasma membrane. This angle may reflect the orientation of the Myo2 tail in nodes.

Cdc15 contains a membrane-binding F-BAR domain at its N terminus (Roberts-Galbraith et al., 2010). The distance from Rlc1 to the N and C terminus of Cdc15 is 67 and 60 nm, respectively (Fig. 6, D and E), which indicates that Cdc15 is close to Mid1 and to the plasma membrane. These distances also suggest that the C terminus of Cdc15 is oriented toward the cell interior.

We investigated the distance between Rlc1 and the N terminus of Myo2 indirectly using Cdc15-tandem Tomato (tdTomato) as a reference because of difficulties in measuring small distances accurately. The distance between Cdc15-tdTomato and GFP-Myo2 is 70 nm (Fig. 6 F). Thus, the distance between the Rlc1 C terminus and the Myo2 N terminus is ~ 10 nm

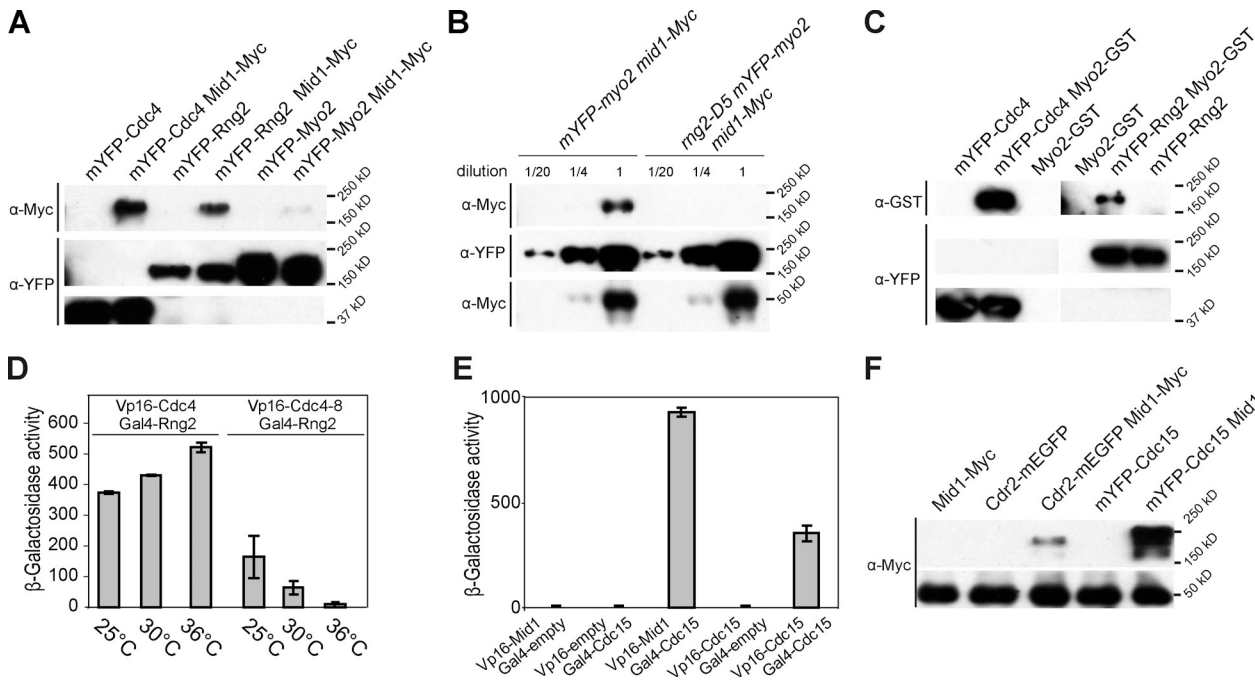


Figure 5. Physical interactions among node proteins revealed by co-IP and yeast two-hybrid assays. (A–C and F) The polyclonal antibody against YFP was used in IP, and all the detected proteins were after IP (see Materials and methods). (A) Mid1 coimmunoprecipitates with Cdc4 and Rng2. The exposure times for Cdc4 and Rng2-Myo2-Mid1 were 5 and 60 s, respectively. Note that no Mid1 was coimmunoprecipitated in the strain expressing Mid1-13Myc alone as shown in Fig. 5 F. (B) Mid1 does not coimmunoprecipitate with Myo2 in the *rng2-D5* strain. wt and *rng2-D5* cells were grown for 4 h at 36°C before protein extractions. Three dilutions of cell extracts were used. The top band is Mid1-Myc, the middle one is mYFP-Myo2, and the bottom is a nonspecific band used as a loading control. (C) Myo2 coimmunoprecipitates with Cdc4 and Rng2. Because of different concentrations of Cdc4 (4.8 μ M) and Rng2 (0.2 μ M) in wt cells (Wu and Pollard, 2005), the exposure time to reveal Cdc4 and Rng2 (α -YFP) was 5 and 30 s, respectively. (D and E) Yeast two-hybrid assays between the indicated constructs. β -Galactosidase activities (means \pm SD) are shown, and the units were defined as $(A_{420} \times 10,000/A_{600})/\text{min.ml}$. Each experiment was repeated twice. (D) The Cdc4-Rng2 interaction is compromised by the *cdc4-8* mutation at different temperatures. (E) Cdc15 interacts with itself and with Mid1. (F) Mid1 coimmunoprecipitates with Cdc15. Cdr2 was used as a positive control, and a nonspecific band was used as a loading control (bottom band).

(compare Fig. 6, E and F), which is consistent with the distances measured for other myosin-IIIs (Shih et al., 2000; Xiao et al., 2003).

Next, we determined that the 2D distance between Myo2-GFP and Rlc1-tdTomato is 42 nm, with the Myo2 C terminus closer to the plasma membrane (Fig. 6 G). The 2D distance between Rng2 and Rlc1 is 47 nm (Fig. 6 H), which suggests that Rng2 is close to the Myo2 tail. The 2D distance between Cdc4 and Rlc1 is 53 nm (Fig. S4 G), which places Cdc4 close to Rng2. Given that Rng2 has ≤ 11 IQ domains (Wang et al., 2004) and a vast excess of Cdc4 in nodes (Table II), we assume that our measurements mainly reflect the Cdc4 fraction that binds to Rng2. Lastly, the 2D distance from Rlc1 to Cdc12 is 63 nm, which places Mid1, Cdc15, and Cdc12 very close to each other in nodes (Figs. 6 J and S4 H). Together, the node architecture is consistent with the protein interactions we discovered and further validates the node assembly pathways (Fig. 3 E).

Lastly, we determined the location of actin filaments relative to the orientation of Myo2 heads by measuring the angles of actin filaments from Cdc12 nodes at the cell sides. Actin filaments/bundles anchored by Cdc12 nodes display a small angle of $8.2 \pm 8.0^\circ$ ($n = 44$ filaments) to the cell's long axis away from the plasma membrane (Fig. 6 I). Given the mean distance between nodes, this small angle suggests that actin filaments could be readily captured by Myo2 heads (Fig. 6 J and see Discussion).

Discussion

Cytokinesis nodes are proposed to be precursors of the contractile ring in fission yeast (Wu et al., 2006; Vavylonis et al., 2008). They are essential for efficient ring assembly, which involves actin filaments and >30 proteins, at the correct cleavage plane (Coffman et al., 2009; Pollard and Wu, 2010). However, little was known about the assembly and architecture of nodes. In animal cells, anillin and myosin-II are enriched in node-like foci (Noguchi et al., 2001; Straight et al., 2003; Werner et al., 2007; Zhou and Wang, 2008). In addition, cytokinesis nodes also resemble the contractile unit of the contractile ring in *Caenorhabditis elegans* (Carvalho et al., 2009). Thus, studying the assembly and architecture of the relatively simple cytokinesis nodes will help us to decipher the much more complex contractile ring during cytokinesis.

Here, we find that cytokinesis nodes are assembled hierarchically, with two modules linked by the anillin-like protein Mid1 in fission yeast (Fig. 3 E). Module I consists of Mid1 recruiting myosin-II essential light chain Cdc4 and IQGAP Rng2, which subsequently binds myosin-II heavy chain Myo2 and regulatory light chain Rlc1. Module II assembles independently at a later stage and consists of Mid1 recruiting F-BAR protein Cdc15. The two modules allow assembly of a compact contractile ring by recruiting actin-nucleating formin Cdc12.

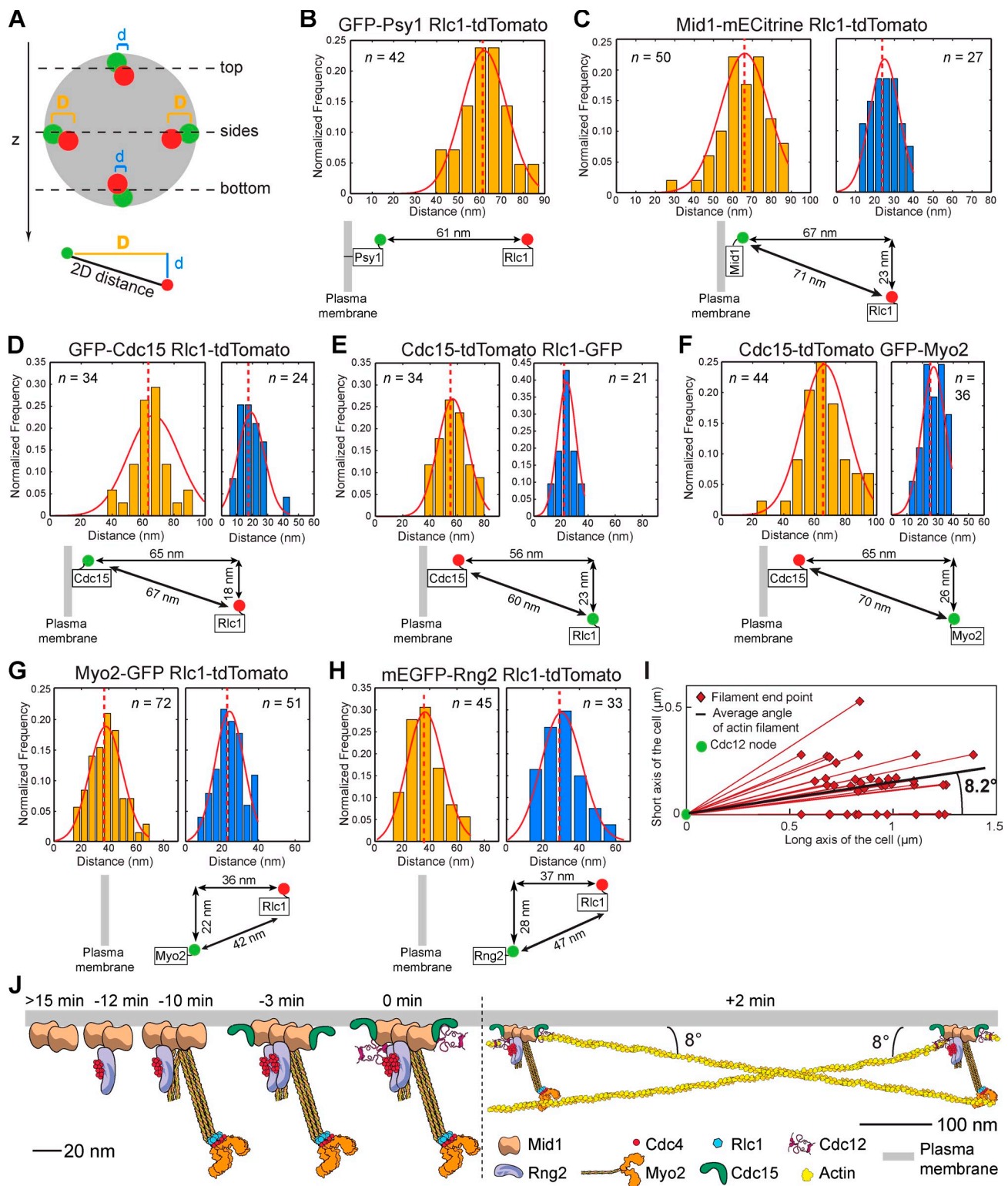


Figure 6. Node architecture revealed by the distances between node proteins. (A) Diagrams of cell sides and cell top and bottom used to measure distances between two proteins tagged with GFP (green dot) and tdTomato (red dot). Distances measured at cell sides are depicted as D and at cell top and bottom as d . After fitting these distances with the non-Gaussian equation, the predicted distances D and d between the two fluorophores were used to calculate the 2D distance using the Pythagorean theorem. (B–H) Non-Gaussian probability distribution fits for protein distance measurements in nodes. Except for GFP-Psy1/Rlc1-tdTomato, each panel contains two graphs representing the histograms of measurements at the cell sides and at cell top and bottom, colored in orange and blue, respectively. The curves are the maximum likelihood fit. Dashed lines represent the distances predicted by maximum likelihood estimation. For each measurement, numbers of analyzed nodes are indicated. The orientation of the protein pair toward the plasma membrane is depicted at the bottom of the graphs. The distances predicted by maximum likelihood estimation (D and d) and the calculated 2D distance are shown along with the orientation. (I) Angles of the GFP-calponin homology domain-marked actin filaments anchored by Cdc12-tdTomato nodes to the long axis of the cell. Only filaments at cell sides were measured. $n = 44$. (J) Model for cytokinesis node assembly and architecture. Protein distances, stoichiometries (except Cdc12), and timings of appearance are depicted.

The anillin Mid1-Cdc4-IQGAP Rng2 module for cytokinesis node assembly

In module I, Mid1, Cdc4, and Rng2 are the stable components to initiate node assembly. Mid1 molecules bind to the plasma membrane as oligomers to form a platform for other proteins to bind (Celton-Morizur et al., 2004). Cdc4 and Rng2 display almost identical recovery rates after photobleaching and identical recruitment kinetics (Fig. 4), which suggest that Cdc4 and Rng2 form a subcomplex and may associate/disassociate from Mid1 together. Once assembled, the Mid1-Cdc4-Rng2 complex recruits dynamic proteins Myo2-Rlc1 and formin Cdc12 to nodes (Fig. 3 E). The dynamic nature of Myo2 and Cdc12 could contribute to contractile ring assembly, as transient interactions between nodes and actin filaments are required during node condensation into a contractile ring (Vavylonis et al., 2008). Rng2, Cdc4, and Cdc15 are more stable in nodes ($t_{1/2} = 1.2\text{--}1.8$ min) than in the contractile ring ($t_{1/2} = 0.3\text{--}0.5$ min; Pelham and Chang, 2002; Clifford et al., 2008; Roberts-Galbraith et al., 2009), which suggests that actin filaments and changes in binding partners in the contractile ring may affect their dynamics. In addition, departure of interphase node proteins from the division site may also make cytokinesis proteins more dynamic, as revealed by our FRAP results in *cdr2Δ* cells (Table II).

Mid1 localization is highly regulated to restrict the division site to the cell equator. Initially, Mid1 is mainly localized in the nucleus. Polo kinase is indicated to phosphorylate and release Mid1 from the nucleus to initiate cytokinesis node formation (Bähler et al., 1998a). Mid1 is maintained as a band of nodes at the cell equator by a balance of positive and negative signals (Celton-Morizur et al., 2006; Padte et al., 2006; Huang et al., 2007; Zhang et al., 2010). Here, we find a novel positive feedback regulation for Mid1 by Cdc4 and Rng2 during cytokinesis node formation (Figs. 2 and 3 E). Consistently, Cdc4 and Rng2 are recruited to nodes when Mid1 level increases to reach the second plateau (Fig. 4 A). Thus, both Mid1 phosphorylation by Polo kinase and binding with Cdc4-Rng2 are involved in doubling the levels of Mid1 in cytokinesis nodes (Fig. 4 A). In mammalian cells, a positive feedback loop also reinforces the localization of anillin at the cleavage site (D'Avino, 2009).

Our finding that Myo2 node localization depends on Rng2 is surprising because it has been proposed that Mid1 recruits Myo2 by binding to the last 133 amino acids of the Myo2 tail, but the tail fragment was overexpressed in the study (Motegi et al., 2004). We did observe a faint band in Myo2-Mid1 IPs when both proteins are expressed at their native levels, which suggests a weak interaction. However, the interaction is not sufficient for Myo2 localization to nodes without Rng2 (Figs. 1, 2, and 5). The localization dependencies and physical interaction between Rng2 and Myo2 suggest that Rng2 recruits Myo2 to nodes or stabilizes the interaction between Myo2 and Mid1.

We find that Rng2, Cdc4, Myo2 tail, and Cdc12 are all close to Mid1 and the plasma membrane, which is consistent with their physical interactions (Figs. 5, 6, and S4). The Myo2 head is ~ 80 nm from Mid1. Interestingly, anillin and myosin-II also do not colocalize perfectly but display a periodic pattern in HeLa cells, suggesting that this architecture may be conserved in animal cells (Straight et al., 2005). Recombinant Myo2 tails

are ~ 87 nm long, and sequence analyses suggest that the tail is folded back (Bezanilla and Pollard, 2000; Motegi et al., 2004), which is consistent with our measurements.

Analysis of node motion and Monte Carlo simulations supports a SCPR model for contractile ring assembly from cytokinesis nodes (Vavylonis et al., 2008). The SCPR model assumed that myosin motors in one node capture and pull actin filaments growing from other nodes. Direct observations and simulations support this assumption. Our data show that actin filaments nucleated by Cdc12 are mostly near the plasma membrane with a small tilt of $\sim 8^\circ$ away from the membrane (Fig. 6 I). Cortical endoplasmic reticulum tubules restrict node movement (Zhang et al., 2010), so they might also confine actin filaments close to the plasma membrane. The distances between nodes are ~ 560 nm. The barbed ends of actin filaments are ~ 80 nm from the Myo2 head in the same node, and the Myo2 tail is oriented at $\sim 70^\circ$ to the plasma membrane. This configuration enables Myo2 heads to capture the pointed ends of actin filaments from neighboring nodes very efficiently (Fig. 6 J). Thus, node architecture is consistent with the SCPR model (Vavylonis et al., 2008). In addition, the distances between Myo2 and other node proteins suggest that the two-headed myosin-II might not be assembled into bipolar filaments (Fig. 6 J). Further studies are needed to determine whether Myo2 assembles and/or aligns into minifilaments during ring maturation and constriction in fission yeast as myosin-II in other systems (Sinard et al., 1989; Mahajan and Pardue, 1996).

The anillin Mid1 and F-BAR protein Cdc15 module for cytokinesis node assembly

Cdc15 appears in nodes later than the proteins in module I but before node condensation. In FRAP assays, Cdc15 exhibits biphasic recovery, with a slow phase ($t_{1/2} = 1.1$ min), supporting its role as a scaffolding protein in nodes to recruit formin Cdc12 by physical interaction (Carnahan and Gould, 2003). The N terminus of Cdc15 lies very close to Mid1, consistent with the physical interactions between Cdc15 and Mid1 (Fig. 5, E and F) as well as Cdc15 and the plasma membrane (Takeda et al., 2004). Although Cdc15 is not required for node and contractile ring assembly, node condensation into a ring is slower, and the ring collapses before constriction without Cdc15 (Wachtler et al., 2006; Hachet and Simanis, 2008). Our data confirms that module I is sufficient to assemble a compact contractile ring. When module I functions normally, Cdc15 is only required for the maturation of the compact ring during anaphase B (Pollard and Wu, 2010).

The interactions between modules I and II and their downstream proteins

The two modules for node assembly can cooperate with each other for successful assembly of the contractile ring in at least four ways: (1) Cdc4 and Rng2 provide a positive feedback for Mid1 recruitment, and Mid1 in turn is essential for the assembly of both modules; (2) both modules are involved in recruiting Cdc12 to nodes; (3) actin filaments nucleated by Cdc12 can recruit and/or bind to Rng2 (Takaine et al., 2009), Myo2, and other actin-binding proteins; (4) Cdc15 physically interacts with

Rng2 (Roberts-Galbraith et al., 2010) and, thus, links the two modules together in the contractile ring.

The interactions between the two modules and their downstream proteins can explain the two overlapping pathways for contractile ring assembly in fission yeast: the Mid1–nodes pathway (Wu et al., 2006; Vavylonis et al., 2008) and the septation initiation network (SIN)–Cdc15 pathway (Wachtler et al., 2006; Hachet and Simanis, 2008). Without Mid1, cells cannot form nodes, and a randomly placed contractile ring is sometimes formed using the SIN–Cdc15 pathway. It takes much longer to form and constrict the misplaced ring (Huang et al., 2008). In *mid1Δ* cells, Cdc15, Cdc4, Rng2, Myo2, Cdc12, and the SIN pathway are all essential for formation of the misplaced contractile ring. Because Cdc15 can bind to the plasma membrane (Takeda et al., 2004), it might anchor or recruit other proteins to the plasma membrane in *mid1* mutants. Then the myosin-II motor and formin Cdc12 could work together to form contractile filaments/bundles and/or a misplaced ring. In the absence of Mid1, Rng2 might be recruited to the plasma membrane by binding to Cdc15 (Roberts-Galbraith et al., 2010) or to the actin filaments nucleated by Cdc12 (Takaine et al., 2009). These multiplex protein interactions among the node proteins may explain the plasticity of contractile ring formation.

Contractile ring assembly in other model systems

Most proteins involved in contractile ring assembly, including the seven node proteins, are conserved during evolution. Step-wise recruitment for ring assembly was described in *S. cerevisiae* and animal cells (Lippincott and Li, 1998; Boyne et al., 2000; Shannon and Li, 2000; Vallen et al., 2000; Luo et al., 2004; Dean et al., 2005; Barr and Gruneberg, 2007). Recently, it has been shown that IQGAP Igq1 recruits myosin-II Myo1 to the contractile ring during cytokinesis in *S. cerevisiae* (Fang et al., 2010). Thus, the localization hierarchy and protein interactions we discovered here may also be conserved in other systems.

Accumulating evidence indicates that anillins function as scaffolding proteins to recruit myosin-II, actin filaments, septins, and other proteins for contractile ring assembly in animal cells (D’Avino, 2009). However, anillins are not essential for cleavage site selection and contractile ring formation (Straight et al., 2005). Redundant pathways for ring assembly may also exist in animal cells as suggested in *C. elegans* embryos (Maddox et al., 2007). Formin CYK-1 is essential for coalescence of myosin-II foci to the cleavage furrow and for cytokinesis in *C. elegans* (Severson et al., 2002; Werner et al., 2007). Although Cdc15-like F-BAR proteins (Spencer et al., 1997) and IQGAP proteins (Nishimura and Mabuchi, 2003; Mondal et al., 2010) are present in animal cells and amoebas, their roles in cytokinesis are not well understood. Thus, our study sheds light on how these proteins might interact and cooperate in cytokinesis.

We conclude that cytokinesis nodes, the precursors for the contractile ring, are assembled in a hierarchical order and link the positional cues for the cleavage site to contractile ring assembly during cytokinesis in fission yeast. Our data provide functional insights and a basis to investigate the contractile ring assembly in other systems.

Materials and methods

Strains, growing conditions, and genetic and cellular methods

Table S1 lists the *S. pombe* strains used in this study. All tagged genes are under the control of endogenous promoters and integrated at their native chromosomal loci. Functionalities of newly tagged strains were tested by examining the growth and morphology at different temperatures and by crossing tagged strains with mutations (Table S1) known to have synthetic interactions with mutations in the tagged genes. Cells were grown in an exponential phase for 36–48 h before microscopy as previously described (Wu et al., 2006). Most temperature-sensitive strains for microscopy were synchronized by growing exponential cultures with 20 mM hydroxyurea (Sigma-Aldrich) for 4 h at 25°C and then 1 h at 36°C. Cells were then washed twice with prewarmed 36°C YE5S medium, and the cell cycle was resumed at 36°C in YE5S for 1 h before imaging at 36°C.

Diploid strains with both copies of the gene for localization analysis tagged with YFP were constructed by standard genetic methods (Moreno et al., 1991). One copy of the essential genes from the diploid strains was deleted using the *KS-ura4*⁺ marker as previously described (Bähler et al., 1998b). Resulting heterozygous diploid strains were grown for 2 d on SPA5S plates to induce sporulation, and then tetrads were inoculated in 2% glusulase for 12 h at 25°C to kill the remaining diploid cells. After five washes in 1.7 g/liter of the rinsing medium (Yeast Nitrogen Base; BD), spores were germinated and grown in YE5S-ura liquid medium at 25°C for 12 or 24 h before imaging. Extra spores were kept at 4°C for repeating experiments. Cells from germinated wt spores were used as controls. The null mutant cells were identified by the failure in contractile ring formation and cytokinesis in time-lapse videos. Because fission yeast diploid cells are not stable for long-term storage, only the parental strains are listed in Table S1.

We constructed the *N-degron-my02* strain as previously described (Rajagopalan et al., 2004) under the control of the *myo2* promoter. The *N-degron-HA* fragment was cloned into the pFA6a plasmid (JQW246). The fragment *kanMX6-Pmyo2-N-degron-HA* flanked with ~70-bp homology to *myo2* was integrated at the *myo2* locus. Positive clones were confirmed by PCR over both junctions.

Microscopy and data analysis

Cells for microscopy were collected from liquid cultures, centrifuged at 5,000 rpm, and then washed into EMM5S for imaging. Live-cell microscopy was performed using a thin layer of EMM5S liquid medium with 20% gelatin (Sigma-Aldrich) and 0.1 mM *n*-propyl-gallate and observed at 23–25°C as previously described (Wu et al., 2006; Coffman et al., 2009). To observe cells at 36°C, cells were spun down for 30 s at 7,000 rpm and placed on EMM5S + 2% agar pads prewarmed for 10 min at 36°C. All slides, coverslips, and cultures were kept at 36°C during preparations of samples to maintain cells at 36°C. An Objective Heater system (Bioptechs) was used to maintain the temperature at 36°C or other temperatures for microscopy of temperature-sensitive mutants. In general, fluorescence intensity was lower at 36°C than at 25°C, making it more difficult to observe nodes in some strains.

For imaging, we used a 100×/1.4 NA objective lens (Nikon) on a spinning-disk confocal microscope (UltraVIEW ERS; PerkinElmer) with a 440-nm solid-state laser, 488-, 514-, and 568-nm argon ion lasers, and a cooled charge-coupled device camera (ORCA-AG; Hamamatsu) with 2 × 2 binning or no binning (for distance measurement). Maximum intensity projections of color images, grayscale montages, and other image analyses were performed using ImageJ (National Institutes of Health). Images in figures are maximum intensity projections of z sections spaced at 0.2–0.8 μm except where noted. For genetic dependencies, the time intervals in time-lapse videos were as follows: 1 min for mYFP-Cdc4 and Rlc1-mYFP; 1.5–2 min for mYFP-Cdc15; and 2 min for Cdc12-3YFP, mYFP-Rng2, YFP-Myo2, and Mid1-monomeric enhanced Citrine (mECitrine).

FRAP analysis

We used the Photokinesis unit on the confocal system (UltraVIEW ERS) for all FRAP experiments (Coffman et al., 2009). The FRAP data were gathered by first taking z sections to determine the optimum cell and plane for bleaching, which contained several nodes whose intensity appeared to have reached the plateau stage and had not started condensation. Then we collected five prebleach images, bleached several nodes in a single plane, and acquired 50 or 100 postbleach images appropriate to the timing of recovery. A region of interest (ROI) was selected at each site that was bleached >50% of the original signal. After subtracting the background and correcting for photobleaching during image acquisition at non-bleached sites (Vavylonis et al., 2008), intensity values at each ROI were

normalized against the mean prebleach value, which was set to 100%. We averaged intensity values of postbleaching from three consecutive images for each ROI to reduce noise (Vavylonis et al., 2008). The averaged value at each time point across all ROIs was plotted as the percentage of recovery with the bleaching time defined as time 0 and the fluorescence intensity after bleaching set to 0%.

Best-fit curves were obtained from the mean of all ROIs and from individual ROIs separately to obtain SDs. The single exponential curve equation used in *KaleidaGraph* software (Synergy Software) is $y = m_1 + m_2 \times \exp(-m_3 \times x)$, in which m_2 is the off rate. The off rate was used to calculate the half-time of the recovery by the equation $t_{1/2} = \ln 2 / m_3$. The variable m_1 is the plateau of the recovery. Some curves were determined to have two phases of recovery by plotting the recovery rates from a single exponential fit, $k_{\text{off}} \times t = -\ln((y_x - m_1) / (y_0 - m_1))$, in which y_0 is the y value at time 0, and y_x is the y value at time x . The resulting curve can be fit with either one or two linear fits, indicating one or two off rates as in Fig. 4 (E and F), in which the slope of each line is k_{off} . Biphasic recovery curves were then fit with the double exponential equation $y = m_1 + m_2 \times \exp(-m_3 \times x) + m_4 \times \exp(-m_5 \times x)$, in which m_3 and m_5 are the off rates for the slow and fast phases, respectively. The contribution of the fast phase to the total recovery is calculated by $m_4 / (y_0 - m_1)$. $m_2 + m_4$ is the difference between the intensity right after bleach and the plateau, such that in a single exponential fit, $y_0 - m_1 = m_2$, whereas in a double exponential fit, $y_0 - m_1 = m_2 + m_4$. Note that m_2 and m_4 are both negative for FRAP fits. To obtain a plateau for each recovery curve, images were collected with different time intervals: a 1-s (*Cdc15* in *cdr2Δ*), 2-s (all *Myo2*, *Cdc4* in *myo2**, *Cdc15* in *cdr2Δ*, and *Rlc1*), 10-s (all *Rng2*, *Cdc4* in *myo2*-*Q1Δ/Q2Δ*, and *Mid1* in *cdr2Δ*), or 20-s delay (*Mid1* interphase nodes).

Counting numbers of molecules during node assembly

We counted molecules in nodes based on fluorescence intensity (Wu and Pollard, 2005) with some modifications. We define one polypeptide as one molecule throughout the paper, except there are three tandem YFP molecules for every *Cdc12* in the *Cdc12-3YFP* fusion polypeptide. For intensity comparison, images were collected using the same laser power and imaging settings. The same strain expressing *Rlc1*-mYFP was imaged at the beginning and end of the experiments to ensure that the laser intensity remained constant.

We used the full width at half-maximum to determine the sampling interval along the *z* axis (Hirschberg et al., 1998; Wu and Pollard, 2005). The full width at half-maximum for our confocal system was 0.44 ± 0.07 nm in the *z* direction. Thus, *z* sections spaced at $0.4 \mu\text{m}$ of strains expressing monomeric EGFP (mEGFP)-tagged *Mid1* were collected for comparing to an EGFP-tagged *MotB* motor in *Escherichia coli*, which is known to contain a mean of 22 molecules (Leake et al., 2006). The *E. coli* strain expressing EGFP-*MotB* (JPA750) was grown in tryptone broth with shaking overnight at 30°C and then washed and suspended in motility buffer (10 mM potassium phosphate and 0.1 mM EDTA, pH 7.0) for imaging as previously reported (Leake et al., 2006). The strain was imaged on bare slides first to verify motility-indicating functional motors. The strain was then imaged on slides with motility buffer containing 20% gelatin for comparison with *Mid1*-mEGFP.

The slight difference in intensity of GFP variants was corrected using strains expressing integrated *Rlc1*-GFP under the control of the native promoter. Comparison between cellular concentrations of *Rlc1*-mEGFP and *Rlc1*-EGFP was performed as previously described (Wu and Pollard, 2005). In brief, offset pixel intensity was subtracted from all images. Then, the images were corrected for uneven illumination. Cell size-corrected pixel intensity in sum images was measured for each strain and for a wt strain with no fluorescent tag ($n = 60$ cells for each strain). Then, the wt autofluorescence intensity was subtracted from both *Rlc1* strains. We found that mEGFP is $1.14 \times$ brighter than EGFP.

We first used EGFP-*MotB* as a standard to quantify the mean numbers of molecules in *Mid1*-mEGFP nodes in a single stack. Offset intensity value from the system was subtracted from each image, and images of purified GFP were used to correct for uneven illumination in the field as previously described (Wu and Pollard, 2005). Intensities of individual nodes in a single stack were measured using a circular ROI in *ImageJ*, and background corrections were made using five equal-sized ROIs from nearby cytoplasmic areas without nodes. The size of each ROI was optimized using Gaussian fits of the signal intensity in the *x*-*y* axis to measure $>90\%$ of the signal. Node intensities were obtained from the sum of two to three consecutive *z* sections. *Mid1* nodes were measured after the signal from the nucleus had disappeared to ensure the measurement of only cytokinesis nodes. Node intensities were divided by 1.14 to correct for the slight difference in

intensity between mEGFP and EGFP and then compared with the intensity of EGFP-*MotB* motors that contain 22 molecules (Leake et al., 2006) to obtain the mean number of *Mid1* molecules in individual nodes.

We next determined the number of all protein molecules in nodes over time. Three *z* sections spaced at $0.2 \mu\text{m}$ were collected every 20 s for 20 min using strains expressing mYFP or 3YFP-tagged node proteins. mYFP is $1.1 \times$ brighter than YFP, and *Cdc12-3YFP* is $3 \times$ brighter than *Cdc12-YFP* (Wu and Pollard, 2005). Photobleaching during image acquisition was corrected. Individual node intensities over time were measured, and background fluorescence from the mean of five nearby ROIs of the same size was subtracted. The slice with a maximum intensity that could be tracked over time was used for measurements. The fraction of signal present in the best focal plane was determined to be 45–55% of the total in each node. Thus, the intensity from the maximum intensity plane was divided by this fraction to obtain the total intensity in nodes. The time of node appearance, except that of *Mid1*, was defined as an intensity $\geq 25\%$ higher than the cytoplasmic background. The timing of the transition for *Mid1* from interphase nodes to cytokinesis nodes was defined as the time that the *Mid1* node signal increased to $\geq 25\%$ higher than that of interphase nodes. The number of molecules in nodes over time was determined by setting the second plateau of *Mid1*-mYFP nodes to 27.7, the value obtained by comparison to *MotB*. The ratios of plateaus of cytokinesis nodes are similar to the numbers counted previously (Wu and Pollard, 2005), validating the method. Before condensation, nodes move very little by diffusion (Vavylonis et al., 2008). Some nodes could be tracked for several minutes even after the beginning of condensation but before merging with other nodes. The time point of the beginning of node condensation is used to align all the nodes temporally. Each data point in the plateaus in Fig. 4 A is the averaged value at each time point after all the nodes appeared.

The time of the beginning of node condensation relative to the SPB separation was measured in the strain expressing GFP-*Myo2* *Sad1*-mEGFP at 25°C , resulting in 2.3 min on average. Thus, the time point at the beginning of node condensation for each cell in the videos for counting molecules was set to 2.3 min so that time 0 represents SPB separation.

IP and immunoblotting

We immunoprecipitated *S. pombe* cell lysates using the polyclonal antibody against YFP [NB600-308; Novus Biologicals] from strains expressing tagged proteins under the control of endogenous promoters and integrated at their native chromosomal loci. 30 μl protein G covalently coupled magnetic Dynabeads (Invitrogen) was washed three times with 1 ml of cold PBS buffer (137 mM NaCl, 2.7 mM KCl, 10 mM Na_2HPO_4 , and 2 mM KH_2PO_4) and then resuspended in 600 μl PBS. 5 μg YFP antibodies was added to the magnetic Dynabeads and incubated for 1 h at 23°C . The antibody-coupled magnetic beads were then washed three times with 1 ml PBS and once with 1 ml 1% NP-40 buffer (50 mM Hepes, pH 7.5, 100 mM NaCl, 1 mM EDTA, 1% NP-40, 50 mM NaF, 20 mM glycerophosphate, and 0.1 mM Na_3VO_4).

30 mg lyophilized cells ($\sim 1.2 \times 10^9$ cells) per sample was resuspended in 300 μl IP buffer (1% NP-40 buffer, 1 mM PMSF, and protease inhibitor [Roche]). Under these conditions, $\sim 50\%$ of the cells were lysed (Liu et al., 2010). After low speed centrifugation at 3,000 rpm for 30 s at 4°C , 200 μl supernatant was centrifuged again at 13,000 rpm for 10 min at 4°C . 130 μl supernatant was transferred to use as a cell lysate. 120 μl lysate was added to the antibody-coupled beads and incubated for 90 min at 4°C . Beads were washed five times with 1 ml of cold 1% NP-40 buffer. In some cases, a more stringent buffer (1% NP-40 buffer with 200 mM NaCl) was used in washing steps. Then, 50 μl sample buffer was added to the beads and boiled for 5 min to elute the proteins. Reciprocal co-IPs were performed using the monoclonal antibody against myc (sc-40 [9E10; Santa Cruz Biotechnology, Inc.]).

Immunoblotting was performed as previously described (Wu and Pollard, 2005) with the following modifications/additions: (a) the following monoclonal antibodies were used to against: myc (sc-40 [9E10; dilution 1:5,000], YFP [632381; 1:5,000 or 1:2,500; Takara Bio Inc.], GST [NB600-446; 1:5,000; Novus Biologicals], and actin (C4 against chicken gizzard actin; 1:2,000; a gift from J. Lessard, University of Cincinnati Children's Hospital, Cincinnati, OH); (b) anti-mouse IgG (A4416; Sigma-Aldrich) was used in a 1:10,000 dilution; (c) blots were reacted with SuperSignal Maximum Sensitivity Substrate (Thermo Fisher Scientific) and exposed to film (BioMax MR; Kodak); (d) to address protein stability (Fig. S2 A), total proteins were extracted using 5% TCA as previously described (Laporte et al., 2008).

In Lat-A treatment experiments (Fig. S2 F), beads after co-IP were washed three times with 1 ml of cold 1% NP-40 buffer and split into two

nonadherent tubes. One tube was incubated with 100 μ M Lat-A, and the other was incubated with equal volume DMSO at room temperature for 5–15 min with shaking. Beads were then collected by the magnetic rack. After removing the supernatant, beads were washed once with 1 ml of cold 1% NP-40 buffer. 50 μ l sample buffer was added to the beads and boiled for 5 min to elute the proteins.

Yeast two-hybrid assays

For two-hybrid assays, *cdc4*, *cdc4-8*, *cdc15*, *mid1*, and *rng2* open reading frames were fused with the VP16 activation domain and *GAL4* DNA-binding domain in JQW270 (*TRP1*, 2 μ m) and JQW271 (*LEU2*, 2 μ m) plasmids, respectively (gifts from J. Hopper, The Ohio State University, Columbus, OH). The *S. cerevisiae* strain MaV203 was used for the assays (11281–011; Invitrogen). β -Galactosidase assays were performed as described in the o-nitrophenyl β -D-galactopyranoside assay (Sigma-Aldrich), and β -galactosidase units were defined as $(A_{420} - 10,000/A_{600})/\text{min}/\text{ml}$.

Measurements of molecular distances in nodes

We measured protein distances in nodes using the SHREC method (Churchman et al., 2005; Joglekar et al., 2009) with some modifications. Measurements were made in strains simultaneously expressing two node proteins tagged with GFP (except mECitrine for Mid1) and tdTomato under the control of their native promoters. The distance between the centroids of GFP and tdTomato reflects the mean distance separating two labeled protein clusters within the same node.

Before each experiment, images of 100-nm TetraSpeck beads (Invitrogen) were acquired for image registration (Fig. S4, A and B). For each strain, 21 z sections spaced at 200 nm were obtained. The exposure times were between 200 and 700 ms per image to maintain a high signal/noise ratio with minimal bleaching during image acquisition. It took 107 ± 2 ms to switch between 488- and 568-nm channels. Thus, node displacements while acquiring one pair of images (took 0.8–1.2 s) were negligible because the diffusion constant of nodes is $\sim 20 \text{ nm}^2/\text{s}$ before node condensation (Vavylonis et al., 2008). We used slices 2–4 and 17–19 to measure the distances at the cell top and bottom (usually there is no node signal in slices 1, 20, and 21) and slices 9–12 to measure the distances at the cell sides as shown in Fig. 6 A.

Image analyses were performed with custom software written in MatLAB R2009 (MathWorks). After determining the offset mapping for a specific location in the field using TetraSpeck beads at concentrations of 80–120 beads/100 μ m 2 , a tdTomato image from the same location was selected and transformed using the local weighted mean algorithm as previously described (Churchman et al., 2005; Joglekar et al., 2009). Then, the same region with cells containing nodes was selected using the corrected tdTomato images and the GFP images. For centroid determination, a 6-pixel square ROI was taken on a tdTomato node image after offset correction (Fig. S4, A and B). The corresponding region from the GFP node image was then extracted. We assumed that the fluorophores are normally distributed in the nodes. Individual GFP/tdTomato node centroids were determined by fitting their intensity distribution with a 2D Gaussian function. We only present data with $R^2 > 0.7$ after fitting both of the fluorophores with a 2D Gaussian. Most data with $R^2 < 0.7$ have very low intensity and are difficult to fit. Using the obtained centroid coordinates, distances between the centroids were determined. Then, the distribution of these distances was fit with a 2D non-Gaussian probability density function. Lastly, 2D distances and angles to the long axis of the cell were calculated using the Pythagorean theorem as described in Fig. 6 A. Measuring distances on cell sides only reveals the projection of the real distance on the imaging plane. To correct this, we also measured the distance at the cell top and bottom to calculate the 2D distance, representing the true distance between the two centroids. This approach obtains a more accurate distance between EGFP and tdTomato centroids.

To determine the distance between Rlc1-tdTomato and the plasma membrane, we used GFP-Psy1, a t-SNARE protein, as a membrane marker. One problem with measuring the distance using GFP-Psy1 is that the Psy1 signal does not form a dot but rather a line along the membrane, making the fit with a 2D Gaussian impossible. We bypassed this problem by fitting a 1D Gaussian with the Psy1 pixel intensity from two parallel lines near the Rlc1 centroid as indicated in Fig. S4 D. The centroids of these two Psy1 fits were used to represent the membrane location. After offset correction, Rlc1 centroid was determined using a 2D Gaussian. The three centroids form a triangle. We defined the length of the altitude from the Rlc1 centroid to the line formed by the two Psy1 centroids as the distance between Rlc1 and the plasma membrane.

Maximum likelihood estimation of the mean centroid distance

We studied the organization of the seven proteins in cytokinesis nodes using a modified version of SHREC (see previous section). The minimum distance that we can measure accurately by our technique was ~ 10 nm, with a confidence interval less than ± 3 nm. If the separation between two protein clusters is equal or smaller than the measurement error, the maximum likelihood method will estimate the mean value of the measurement error rather than the expected distance between the two fluorophores (Joglekar et al., 2009). The physical size of the fluorescent proteins was neglected from our analysis because both ~ 4 -nm EGFP and tdTomato are linked via a short flexible linker to the protein of interest, making it difficult to correct the distance uniformly between each pair of node proteins. We estimated the distances between two proteins in nodes as previously described (Joglekar et al., 2009). The distance measurement for two centroids defined by a 2D Gaussian probability distribution is distributed according to a non-Gaussian distribution probability density function given by (Churchman et al., 2006): $P_{2D}(r) = (r/\sigma^2) \times \exp(-[r^2 + r^2]/2\sigma^2) \times I_0(r\mu/\sigma^2)$, in which r is the distance measured, μ is the true distance between the two fluorophores, σ is the SD for the measured distances, and I_0 is the modified Bessel function of order 0.

It has been shown that the true distance (μ) is more accurate by fitting a dataset to the aforementioned equation instead of calculating the mean value or fitting the data with a Gaussian distribution probability density function (Churchman et al., 2006). To correctly determine μ using this method, the distances measured between two centroids must be normally distributed. In our study, distances between the two centroids do not reflect a single molecule but a cluster of fluorophores, and we assumed that the centroid localization for the cluster of fluorophores should be a Gaussian distribution. Measurement errors (offset introduced by the channel registration and noise caused by the centroid localization of the fluorophores) become a significant factor when distances are measured at a nanometer scale (Fig. S4). The aforementioned equation takes these experimental errors into account. Thus, for any given error, the distribution is asymmetric with a true distance (r) always deviated from the distribution's maximum.

Online supplemental material

Fig. S1 shows that Myo2 recruits Rlc1, but not Rng2, to cytokinesis nodes. Fig. S2 shows protein levels and clump formation in mutants. Fig. S3 shows that Cdc4, Rng2, Myo2, and Mid1 localize to cytokinesis nodes independently of Cdc15 and Cdc12. Fig. S4 shows offset correction, the expected precision in the distance measurement, and the orientation of the node proteins relative to the plasma membrane while also presenting distances from Cdc4, Cdc12, and Myo2 to Rlc1. Table S1 lists the strains used in this study. Online supplemental material is available at <http://www.jcb.org/cgi/content/full/jcb.201008171/DC1>.

We thank Ajit Joglekar and Dimitrios Vavylonis for help with SHREC; Mohan Balasubramanian, Damien Brunner, Fred Chang, Kathleen Gould, James Hopper, Matthew Lord, Dannel McCollum, James Moseley, Paul Nurse, Stephen Osmani, Thomas Pollard, John Pringle, and Viesturs Simanis for strains, plasmids, or equipment; and Stephen Osmani, Arthur Burghes, James Hopper, Susan Burghes, and Aurelie Massoni-Laporte for critical reading of the manuscript. We also thank anonymous reviewers and members of the Wu laboratory for insightful and helpful suggestions and comments.

V.C. Coffman is supported by a predoctoral fellowship from the American Heart Association. This work was supported by the American Heart Association, Great Rivers Affiliate; the Basil O'Connor Starter Scholar Research Award; and the National Institutes of Health grant GM086546 to J.-Q. Wu.

Submitted: 30 August 2010

Accepted: 22 February 2011

References

- Almonacid, M., J.B. Moseley, J. Janvore, A. Mayeux, V. Fraisier, P. Nurse, and A. Paoletti. 2009. Spatial control of cytokinesis by Cdr2 kinase and Mid1/anillin nuclear export. *Curr. Biol.* 19:961–966. doi:10.1016/j.cub.2009.04.024
- Bähler, J., A.B. Steever, S. Wheatley, Y. Wang, J.R. Pringle, K.L. Gould, and D. McCollum. 1998a. Role of polo kinase and Mid1p in determining the site of cell division in fission yeast. *J. Cell Biol.* 143:1603–1616. doi:10.1083/jcb.143.6.1603
- Bähler, J., J.Q. Wu, M.S. Longtine, N.G. Shah, A. McKenzie III, A.B. Steever, A. Wach, P. Philippse, and J.R. Pringle. 1998b. Heterologous modules for efficient and versatile PCR-based gene targeting in

Schizosaccharomyces pombe. *Yeast*. 14:943–951. doi:10.1002/(SICI)1097-0061(199807)14:10<943::AID-YEA292>3.0.CO;2-Y

Balasubramanian, M.K., E. Bi, and M. Glotzer. 2004. Comparative analysis of cytokinesis in budding yeast, fission yeast and animal cells. *Curr. Biol.* 14:R806–R818. doi:10.1016/j.cub.2004.09.022

Barr, F.A., and U. Gruneberg. 2007. Cytokinesis: placing and making the final cut. *Cell*. 131:847–860. doi:10.1016/j.cell.2007.11.011

Bathe, M., and F. Chang. 2010. Cytokinesis and the contractile ring in fission yeast: towards a systems-level understanding. *Trends Microbiol.* 18:38–45. doi:10.1016/j.tim.2009.10.002

Bezanilla, M., and T.D. Pollard. 2000. Myosin-II tails confer unique functions in *Schizosaccharomyces pombe*: characterization of a novel myosin-II tail. *Mol. Biol. Cell*. 11:79–91.

Boyne, J.R., H.M. Yosuf, P. Bieganowski, C. Brenner, and C. Price. 2000. Yeast myosin light chain, Mlc1p, interacts with both IQGAP and class II myosin to effect cytokinesis. *J. Cell Sci.* 113:4533–4543.

Bringmann, H., and A.A. Hyman. 2005. A cytokinesis furrow is positioned by two consecutive signals. *Nature*. 436:731–734. doi:10.1038/nature03823

Carnahan, R.H., and K.L. Gould. 2003. The PCH family protein, Cdc15p, recruits two F-actin nucleation pathways to coordinate cytokinetic actin ring formation in *Schizosaccharomyces pombe*. *J. Cell Biol.* 162:851–862. doi:10.1083/jcb.200305012

Carvalho, A., A. Desai, and K. Oegema. 2009. Structural memory in the contractile ring makes the duration of cytokinesis independent of cell size. *Cell*. 137:926–937. doi:10.1016/j.cell.2009.03.021

Celton-Morizur, S., N. Bordes, V. Fraisier, P.T. Tran, and A. Paoletti. 2004. C-terminal anchoring of mid1p to membranes stabilizes cytokinetic ring position in early mitosis in fission yeast. *Mol. Cell. Biol.* 24:10621–10635. doi:10.1128/MCB.24.24.10621-10635.2004

Celton-Morizur, S., V. Racine, J.B. Sibarita, and A. Paoletti. 2006. Pom1 kinase links division plane position to cell polarity by regulating Mid1p cortical distribution. *J. Cell Sci.* 119:4710–4718. doi:10.1242/jcs.03261

Churchman, L.S., Z. Okten, R.S. Rock, J.F. Dawson, and J.A. Spudich. 2005. Single molecule high-resolution colocalization of Cy3 and Cy5 attached to macromolecules measures intramolecular distances through time. *Proc. Natl. Acad. Sci. USA*. 102:1419–1423. doi:10.1073/pnas.0409487102

Churchman, L.S., H. Flyvbjerg, and J.A. Spudich. 2006. A non-Gaussian distribution quantifies distances measured with fluorescence localization techniques. *Biophys. J.* 90:668–671. doi:10.1529/biophysj.105.065599

Clifford, D.M., B.A. Wolfe, R.H. Roberts-Galbraith, W.H. McDonald, J.R. Yates III, and K.L. Gould. 2008. The Cdc1/Cdc14 phosphatase contributes to the robustness of cytokinesis by association with anillin-related Mid1. *J. Cell Biol.* 181:79–88. doi:10.1083/jcb.200709060

Coffman, V.C., A.H. Nile, I.J. Lee, H. Liu, and J.Q. Wu. 2009. Roles of formin nodes and myosin motor activity in Mid1p-dependent contractile-ring assembly during fission yeast cytokinesis. *Mol. Biol. Cell*. 20:5195–5210. doi:10.1091/mbc.E09-05-0428

D'Avino, P.P. 2009. How to scaffold the contractile ring for a safe cytokinesis - lessons from Anillin-related proteins. *J. Cell Sci.* 122:1071–1079. doi:10.1242/jcs.034785

Dean, S.O., S.L. Rogers, N. Stuurman, R.D. Vale, and J.A. Spudich. 2005. Distinct pathways control recruitment and maintenance of myosin II at the cleavage furrow during cytokinesis. *Proc. Natl. Acad. Sci. USA*. 102:13473–13478. doi:10.1073/pnas.0506810102

D'souza, V.M., N.I. Naqvi, H. Wang, and M.K. Balasubramanian. 2001. Interactions of Cdc4p, a myosin light chain, with IQ-domain containing proteins in *Schizosaccharomyces pombe*. *Cell Struct. Funct.* 26:555–565. doi:10.1247/csf.26.555

Fang, X., J. Luo, R. Nishihama, C. Wloka, C. Dravis, M. Travaglia, M. Iwase, E.A. Vallen, and E. Bi. 2010. Biphasic targeting and cleavage furrow ingress directed by the tail of a myosin II. *J. Cell Biol.* 191:1333–1350. doi:10.1083/jcb.201005134

Hachet, O., and V. Simanis. 2008. Mid1p/anillin and the septation initiation network orchestrate contractile ring assembly for cytokinesis. *Genes Dev.* 22:3205–3216. doi:10.1101/gad.1697208

Hales, K.G., E. Bi, J.Q. Wu, J.C. Adam, I.C. Yu, and J.R. Pringle. 1999. Cytokinesis: an emerging unified theory for eukaryotes? *Curr. Opin. Cell Biol.* 11:717–725. doi:10.1016/S0955-0674(99)00042-3

Hirschberg, K., C.M. Miller, J. Ellenberg, J.F. Presley, E.D. Siggia, R.D. Phair, and J. Lippincott-Schwartz. 1998. Kinetic analysis of secretory protein traffic and characterization of golgi to plasma membrane transport intermediates in living cells. *J. Cell Biol.* 143:1485–1503. doi:10.1083/jcb.143.6.1485

Huang, Y., T.G. Chew, W. Ge, and M.K. Balasubramanian. 2007. Polarity determinants Tea1p, Tea4p, and Pom1p inhibit division-septum assembly at cell ends in fission yeast. *Dev. Cell.* 12:987–996. doi:10.1016/j.devcel.2007.03.015

Huang, Y., H. Yan, and M.K. Balasubramanian. 2008. Assembly of normal actomyosin rings in the absence of Mid1p and cortical nodes in fission yeast. *J. Cell Biol.* 183:979–988. doi:10.1083/jcb.200806151

Joglekar, A.P., K. Bloom, and E.D. Salmon. 2009. In vivo protein architecture of the eukaryotic kinetochore with nanometer scale accuracy. *Curr. Biol.* 19:694–699. doi:10.1016/j.cub.2009.02.056

Kovar, D.R., J.R. Kuhn, A.L. Tichy, and T.D. Pollard. 2003. The fission yeast cytokinesis formin Cdc12p is a barbed end actin filament capping protein gated by profilin. *J. Cell Biol.* 161:875–887. doi:10.1083/jcb.200211078

Laporte, D., B. Salin, B. Daignan-Fornier, and I. Sagot. 2008. Reversible cytoplasmic localization of the proteasome in quiescent yeast cells. *J. Cell Biol.* 181:737–745. doi:10.1083/jcb.200711154

Leake, M.C., J.H. Chandler, G.H. Wadham, F. Bai, R.M. Berry, and J.P. Armitage. 2006. Stoichiometry and turnover in single, functioning membrane protein complexes. *Nature*. 443:355–358. doi:10.1038/nature05135

Le Goff, X., F. Motegi, E. Salimova, I. Mabuchi, and V. Simanis. 2000. The *S. pombe* rlc1 gene encodes a putative myosin regulatory light chain that binds the type II myosins myo3p and myo2p. *J. Cell Sci.* 113:4157–4163.

Lippincott, J., and R. Li. 1998. Sequential assembly of myosin II, an IQGAP-like protein, and filamentous actin to a ring structure involved in budding yeast cytokinesis. *J. Cell Biol.* 140:355–366. doi:10.1083/jcb.140.2.355

Liu, H.L., A.H. Osmani, L. Ukil, S. Son, S. Markossian, K.F. Shen, M. Govindaraghavan, A. Varadaraj, S.B. Hashmi, C.P. De Souza, and S.A. Osmani. 2010. Single-step affinity purification for fungal proteomics. *Eukaryot. Cell.* 9:831–833. doi:10.1128/EC.00032-10

Lord, M., and T.D. Pollard. 2004. UCS protein Rng3p activates actin filament gliding by fission yeast myosin-II. *J. Cell Biol.* 167:315–325. doi:10.1083/jcb.200404045

Luo, J., E.A. Vallen, C. Dravis, S.E. Tcheperegine, B. Drees, and E. Bi. 2004. Identification and functional analysis of the essential and regulatory light chains of the only type II myosin Myo1p in *Saccharomyces cerevisiae*. *J. Cell Biol.* 165:843–855. doi:10.1083/jcb.200401040

Maddox, A.S., L. Lewellyn, A. Desai, and K. Oegema. 2007. Anillin and the septins promote asymmetric ingress of the cytokinetic furrow. *Dev. Cell.* 12:827–835. doi:10.1016/j.devcel.2007.02.018

Mahajan, R.K., and J.D. Pardee. 1996. Assembly mechanism of *Dictyostelium* myosin II: regulation by K^+ , Mg^{2+} , and actin filaments. *Biochemistry*. 35:15504–15514. doi:10.1021/bi9618981

Martin, S.G., and M. Berthelot-Grosjean. 2009. Polar gradients of the DYRK-family kinase Pom1 couple cell length with the cell cycle. *Nature*. 459: 852–856. doi:10.1038/nature08054

Mishra, M., and S. Olierenko. 2008. Cytokinesis: catch and drag. *Curr. Biol.* 18:R247–R250. doi:10.1016/j.cub.2008.01.029

Mondal, S., B. Burgute, D. Rieger, R. Müller, F. Rivero, J. Faix, M. Schleicher, and A.A. Noegel. 2010. Regulation of the actin cytoskeleton by an interaction of IQGAP related protein GAPA with filamin and cortexillin I. *PLoS ONE*. 5:e15440. doi:10.1371/journal.pone.0015440

Moreno, S., A. Klar, and P. Nurse. 1991. Molecular genetic analysis of fission yeast *Schizosaccharomyces pombe*. *Methods Enzymol.* 194:795–823. doi:10.1016/0076-6879(91)94059-L

Moseley, J.B., A. Mayeux, A. Paoletti, and P. Nurse. 2009. A spatial gradient coordinates cell size and mitotic entry in fission yeast. *Nature*. 459:857–860. doi:10.1038/nature08074

Motegi, F., K. Nakano, and I. Mabuchi. 2000. Molecular mechanism of myosin-II assembly at the division site in *Schizosaccharomyces pombe*. *J. Cell Sci.* 113:1813–1825.

Motegi, F., M. Mishra, M.K. Balasubramanian, and I. Mabuchi. 2004. Myosin-II reorganization during mitosis is controlled temporally by its dephosphorylation and spatially by Mid1 in fission yeast. *J. Cell Biol.* 165:685–695. doi:10.1083/jcb.200402097

Mulvihill, D.P., C. Barretto, and J.S. Hyams. 2001. Localization of fission yeast type II myosin, Myo2, to the cytokinetic actin ring is regulated by phosphorylation of a C-terminal coiled-coil domain and requires a functional septation initiation network. *Mol. Biol. Cell*. 12:4044–4053.

Naqvi, N.I., K.C. Wong, X. Tang, and M.K. Balasubramanian. 2000. Type II myosin regulatory light chain relieves auto-inhibition of myosin-heavy-chain function. *Nat. Cell Biol.* 2:855–858. doi:10.1038/35041107

Nishimura, Y., and I. Mabuchi. 2003. An IQGAP-like protein is involved in actin assembly together with Cdc42 in the sea urchin egg. *Cell Motil. Cytoskeleton*. 56:207–218. doi:10.1002/cm.10146

Noguchi, T., R. Arai, F. Motegi, K. Nakano, and I. Mabuchi. 2001. Contractile ring formation in *Xenopus* egg and fission yeast. *Cell Struct. Funct.* 26:545–554. doi:10.1247/csf.26.545

Padte, N.N., S.G. Martin, M. Howard, and F. Chang. 2006. The cell-end factor pom1p inhibits mid1p in specification of the cell division plane in fission yeast. *Curr. Biol.* 16:2480–2487. doi:10.1016/j.cub.2006.11.024

Paoletti, A., and F. Chang. 2000. Analysis of mid1p, a protein required for placement of the cell division site, reveals a link between the nucleus and the cell surface in fission yeast. *Mol. Biol. Cell.* 11:2757–2773.

Pelham, R.J. Jr., and F. Chang. 2002. Actin dynamics in the contractile ring during cytokinesis in fission yeast. *Nature*. 419:82–86. doi:10.1038/nature00999

Pollard, T.D., and J.Q. Wu. 2010. Understanding cytokinesis: lessons from fission yeast. *Nat. Rev. Mol. Cell Biol.* 11:149–155. doi:10.1038/nrm2834

Rajagopalan, S., Z. Liling, J. Liu, and M. Balasubramanian. 2004. The N-degron approach to create temperature-sensitive mutants in *Schizosaccharomyces pombe*. *Methods*. 33:206–212. doi:10.1016/j.ymeth.2003.11.015

Roberts-Galbraith, R.H., and K.L. Gould. 2008. Stepping into the ring: the SIN takes on contractile ring assembly. *Genes Dev.* 22:3082–3088. doi:10.1101/gad.174890

Roberts-Galbraith, R.H., J.S. Chen, J. Wang, and K.L. Gould. 2009. The SH3 domains of two PCH family members cooperate in assembly of the *Schizosaccharomyces pombe* contractile ring. *J. Cell Biol.* 184:113–127. doi:10.1083/jcb.200806044

Roberts-Galbraith, R.H., M.D. Ohi, B.A. Ballif, J.S. Chen, I. McLeod, W.H. McDonald, S.P. Gygi, J.R. Yates III, and K.L. Gould. 2010. Dephosphorylation of F-BAR protein Cdc15 modulates its conformation and stimulates its scaffolding activity at the cell division site. *Mol. Cell.* 39:86–99. doi:10.1016/j.molcel.2010.06.012

Severson, A.F., D.L. Baillie, and B. Bowerman. 2002. A Formin Homology protein and a profilin are required for cytokinesis and Arp2/3-independent assembly of cortical microfilaments in *C. elegans*. *Curr. Biol.* 12:2066–2075. doi:10.1016/S0960-9822(02)01355-6

Shannon, K.B., and R. Li. 2000. A myosin light chain mediates the localization of the budding yeast IQGAP-like protein during contractile ring formation. *Curr. Biol.* 10:727–730. doi:10.1016/S0960-9822(00)00539-X

Shih, W.M., Z. Gryczynski, J.R. Lakowicz, and J.A. Spudich. 2000. A FRET-based sensor reveals large ATP hydrolysis-induced conformational changes and three distinct states of the molecular motor myosin. *Cell*. 102:683–694. doi:10.1016/S0092-8674(00)00090-8

Sinard, J.H., W.F. Stafford, and T.D. Pollard. 1989. The mechanism of assembly of *Acanthamoeba* myosin-II minifilaments: minifilaments assemble by three successive dimerization steps. *J. Cell Biol.* 109:1537–1547. doi:10.1083/jcb.109.4.1537

Sohrmann, M., C. Fankhauser, C. Brodbeck, and V. Simanis. 1996. The *dmf1/mid1* gene is essential for correct positioning of the division septum in fission yeast. *Genes Dev.* 10:2707–2719. doi:10.1101/gad.10.21.2707

Spencer, S., D. Dowbenko, J. Cheng, W. Li, J. Brush, S. Utzig, V. Simanis, and L.A. Lasky. 1997. PSTPIP: a tyrosine phosphorylated cleavage furrow-associated protein that is a substrate for a PEST tyrosine phosphatase. *J. Cell Biol.* 138:845–860. doi:10.1083/jcb.138.4.845

Straight, A.F., A. Cheung, J. Limouze, I. Chen, N.J. Westwood, J.R. Sellers, and T.J. Mitchison. 2003. Dissecting temporal and spatial control of cytokinesis with a myosin II Inhibitor. *Science*. 299:1743–1747. doi:10.1126/science.1081412

Straight, A.F., C.M. Field, and T.J. Mitchison. 2005. Anillin binds nonmuscle myosin II and regulates the contractile ring. *Mol. Biol. Cell.* 16:193–201. doi:10.1091/mbc.E04-08-0758

Sutton, R.B., D. Fasshauer, R. Jahn, and A.T. Brunger. 1998. Crystal structure of a SNARE complex involved in synaptic exocytosis at 2.4 Å resolution. *Nature*. 395:347–353. doi:10.1038/26412

Takaine, M., O. Numata, and K. Nakano. 2009. Fission yeast IQGAP arranges actin filaments into the cytokinetic contractile ring. *EMBO J.* 28:3117–3131. doi:10.1038/embj.2009.252

Takeda, T., T. Kawate, and F. Chang. 2004. Organization of a sterol-rich membrane domain by cdc15p during cytokinesis in fission yeast. *Nat. Cell Biol.* 6:1142–1144. doi:10.1038/ncb1189

Vallen, E.A., J. Caviston, and E. Bi. 2000. Roles of Hof1p, Bni1p, Bnr1p, and myo1p in cytokinesis in *Saccharomyces cerevisiae*. *Mol. Biol. Cell.* 11:593–611.

Vavylonis, D., J.Q. Wu, S. Hao, B. O'Shaughnessy, and T.D. Pollard. 2008. Assembly mechanism of the contractile ring for cytokinesis by fission yeast. *Science*. 319:97–100. doi:10.1126/science.1151086

Wachtler, V., Y. Huang, J. Karagiannis, and M.K. Balasubramanian. 2006. Cell cycle-dependent roles for the FCH-domain protein Cdc15p in formation of the actomyosin ring in *Schizosaccharomyces pombe*. *Mol. Biol. Cell.* 17:3254–3266. doi:10.1091/mbc.E05-11-1086

Wang, C.H., M.K. Balasubramanian, and T. Dokland. 2004. Structure, crystal packing and molecular dynamics of the calponin-homology domain of *Schizosaccharomyces pombe* Rng2. *Acta Crystallogr. D Biol. Crystallogr.* 60:1396–1403. doi:10.1107/S0907444904012983

Werner, M., E. Munro, and M. Glotzer. 2007. Astral signals spatially bias cortical myosin recruitment to break symmetry and promote cytokinesis. *Curr. Biol.* 17:1286–1297. doi:10.1016/j.cub.2007.06.070

Wu, J.Q., and T.D. Pollard. 2005. Counting cytokinesis proteins globally and locally in fission yeast. *Science*. 310:310–314. doi:10.1126/science.1113230

Wu, J.Q., J.R. Kuhn, D.R. Kovar, and T.D. Pollard. 2003. Spatial and temporal pathway for assembly and constriction of the contractile ring in fission yeast cytokinesis. *Dev. Cell.* 5:723–734. doi:10.1016/S1534-5807(03)00324-1

Wu, J.Q., V. Sirotnik, D.R. Kovar, M. Lord, C.C. Beltzner, J.R. Kuhn, and T.D. Pollard. 2006. Assembly of the cytokinetic contractile ring from a broad band of nodes in fission yeast. *J. Cell Biol.* 174:391–402. doi:10.1083/jcb.200602032

Xiao, M., J.G. Reifenberger, A.L. Wells, C. Baldacchino, L.Q. Chen, P. Ge, H.L. Sweeney, and P.R. Selvin. 2003. An actin-dependent conformational change in myosin. *Nat. Struct. Biol.* 10:402–408. doi:10.1038/nsb916

Zhang, D., A. Vjestica, and S. Olierenko. 2010. The cortical ER network limits the permissive zone for actomyosin ring assembly. *Curr. Biol.* 20:1029–1034. doi:10.1016/j.cub.2010.04.017

Zhou, M., and Y.L. Wang. 2008. Distinct pathways for the early recruitment of myosin II and actin to the cytokinetic furrow. *Mol. Biol. Cell.* 19:318–326. doi:10.1091/mbc.E07-08-0783